

This is the peer reviewed version of the following article: Amaral, J. H. F., Melack, J. M., Barbosa, P. M., MacIntyre, S., Kasper, D., Cortés, A., et al. (2020). Carbon dioxide fluxes to the atmosphere from waters within flooded forests in the Amazon basin. *Journal of Geophysical Research: Biogeosciences*, 125, e2019JG005293, which has been published in final form at <https://doi.org/10.1029/2019JG005293>. This article may be used for non-commercial purposes in accordance with Wiley Terms and Conditions for self-archiving.

1 **Carbon dioxide fluxes to the atmosphere from waters within flooded forests in the** 2 **Amazon basin**

3 Joao Henrique Fernandes Amaral^{1,2}, John M. Melack¹, Pedro Maia Barbosa¹, Sally
4 MacIntyre¹, Daniele Kasper³, Alicia Cortés¹, Thiago Sanna Freire Silva⁴, Rodrigo Nunes
5 de Sousa² and Bruce R. Forsberg²

6 ¹ Earth Research Institute, University of California, Santa Barbara, California

7 ² Laboratório de Ecossistemas Aquáticos, Instituto Nacional de Pesquisas da
8 Amazônia, Manaus, Amazonas, Brazil

9 ³ Instituto de Biofísica Carlos Chagas Filho, Universidade Federal do Rio de Janeiro,
10 Rio de Janeiro, Rio de Janeiro, Brazil

11 ⁴ Biological and Environmental Sciences, Faculty of Natural Sciences, University of
12 Stirling, Stirling, UK.

13 Corresponding author: Joao Henrique Fernandes Amaral (jh.amaral@gmail.com)

14 **Key Points:**

- 15 - CO₂ concentrations in near-surface waters within flooded Amazon forests ranged
16 from 19 to 329 μM, and CO₂ fluxes from -0.8 to 55 mmol m⁻² h⁻¹.
- 17 - Daytime CO₂ fluxes were higher at a wind protected site, while night-time fluxes
18 were often higher at a wind exposed site.
- 19 - On an areal basis CO₂ fluxes from flooded forests during high water levels are
20 the major contributor among aquatic habitats

22 **Abstract**

23 Inundated tropical forests are under-represented in analyses of the global carbon
24 cycle and constitute 80% of the surface area of aquatic environments in the lowland
25 Amazon basin. Diel variations in CO₂ concentrations and exchanges with the
26 atmosphere were investigated from August 2014 to September 2016 in two flooded
27 forests sites with different wind exposure within the central Amazon floodplain (3°23' S;
28 60°18' W). CO₂ profiles and estimates of air-water gas exchange were combined with
29 ancillary environmental measurements. Surface CO₂ concentrations ranged from 19 to
30 329 μM, CO₂ fluxes ranged from -0.8 to 55 mmol m⁻² h⁻¹ and gas transfer velocities
31 ranged from 0.2 to 17 cm h⁻¹. CO₂ concentrations and fluxes were highest during the
32 high water period. CO₂ fluxes were three times higher at a site with more wind exposure
33 (WE) compared to one with less exposure (WP). Emissions were higher at the WP site
34 during the day, whereas they were higher at night at the WE site due to vertical mixing.
35 CO₂ concentrations and fluxes were lower at the WP site following an extended period
36 of exceptionally low water. The CO₂ flux from the water in the flooded forest was about
37 half of the net primary production of the forest estimated from the literature. Mean daily
38 fluxes measured in our study (182 ± 247 mmol m⁻² d⁻¹) are higher than or similar to the
39 few other measurements in waters within tropical and subtropical flooded forests and
40 highlight the importance of flooded forests in carbon budgets.

41

42

43

44

45

46

47 **Plain Language Summary**

48 Aquatic habitats in the lowland Amazon emit large quantities of carbon dioxide (CO₂).
49 However, information on CO₂ fluxes from seasonally flooded forests that constitute 80%
50 of the surface area of aquatic environments in the lowland Amazon basin is sparse. We
51 provide the first multi-year measurements of CO₂ exchanges within flooded forests of
52 the central Amazon basin. Our approach combines measurement of dissolved CO₂
53 concentrations and fluxes between the water and atmosphere and ecological data.
54 Although the rates of CO₂ emission by flooded forests are lower than other aquatic
55 habitats, such as open waters in rivers and lakes, the combination of high CO₂
56 concentrations and a large area results in an appreciable regional out-gassing of carbon
57 dioxide from flooded forests. These fluxes can represent about half of the net primary
58 production of flooded forests in the central Amazon basin.

59

60

61 **Keywords:** tropical, CO₂ evasion, wetlands, floodplains

62

63

64

65

66

67

68

69

70 **1. Introduction**

71 Recent syntheses of carbon processing and evasion to the atmosphere from inland
72 aquatic ecosystems have revealed the disproportionately large contribution, relative to
73 their area, that these ecosystems make to carbon cycling and the importance of
74 outgassing of carbon dioxide (Lehner & Döll, 2004; Cole et al., 2007; Raymond et al.,
75 2013). Tropical freshwater systems are under-represented in these analyses, and
76 seasonally inundated forests are seldom considered. Within the lowland Amazon basin,
77 seasonally inundated and riparian forests cover approximately 750,000 km², 15% of the
78 whole lowland area, and are important to the ecology and biogeochemistry of the region
79 (Junk et al., 2010; Melack & Hess, 2010). Floodplain forests occur in an aquatic
80 terrestrial transition zone (ATTZ) (Junk et al., 1989) and are inundated for varying
81 portions of the year depending on water level and local topography (Wittmann et al.,
82 2010). Inundated forests and other floodplain habitats add organic carbon and dissolved
83 CO₂ to floodplains and rivers (Worbes, 1997; Melack & Forsberg, 2001; Melack &
84 Engle, 2009), and contribute to evasion of CO₂ and methane from these aquatic
85 environments (Richey et al., 2002; Melack et al., 2004; Abril et al., 2014; Melack, 2016;
86 Pangala et al., 2017). However, almost all studies of CO₂ outgassing from Amazon
87 floodplains have been restricted to open water areas.

88 CO₂ exchanges with the atmosphere are determined by the gradient of water-air
89 CO₂ concentrations and by the gas transfer velocity (k), a function of turbulence at the
90 air-water interface (MacIntyre et al., 1995; Zappa et al., 2007). Most computations of
91 carbon fluxes from lakes and wetlands use simple wind-based equations of k , though
92 other mechanisms are recognized as important in tropical, temperate and arctic lakes

93 (MacIntyre & Melack 1995; MacIntyre et al., 2002; Tedford et al., 2014; MacIntyre et al.,
94 2018), as well as wetlands (Poindexter et al., 2016). Vegetated aquatic habitats, such
95 as flooded forests, are likely to experience lower wind speeds than open water areas.
96 However, diel variations in cooling or heating of surface waters and associated
97 horizontal water motions and convective mixing can enhance gas exchange even at low
98 wind speeds (MacIntyre et al., 2019). Direct measurements of k , water-air CO₂
99 concentration gradients, and meteorological parameters in flooded forests are needed
100 to better understand the mechanisms associated with CO₂ outgassing from these
101 aquatic habitats and to evaluate their role in the carbon cycle.

102 The first regional estimate of CO₂ outgassing for the aquatic habitats of the Amazon
103 basin (Richey et al., 2002) reported CO₂ outgassing of 830 ± 240 Mg C km⁻² y⁻¹.
104 Subsequent measurements conducted in lakes (Rudorff et al., 2011; Polsenaere et al.,
105 2013), reservoirs (Kemenes et al., 2011) and rivers (Alin et al., 2011; Rasera et al.,
106 2013; Sawakuchi et al., 2017) reported higher k values compared to the values used by
107 Richey et al. (2002). Although seasonally flooded forests can cover large areas, data on
108 k and CO₂ concentrations and fluxes in these habitats are lacking and likely are different
109 from the conditions in the lakes, reservoirs and rivers.

110 Our study contributes to understanding of Amazon floodplains and regional
111 carbon cycling. We provide new information on CO₂ dynamics in inundated forests, the
112 largest aquatic habitat in the Amazon basin, but the one least studied. We report CO₂
113 concentrations, evasion rates and gas transfer velocities measured in flooded forests
114 fringing a floodplain lake along the Solimões River as function of seasonal changes in
115 water depth and day to night differences over the course of two distinct hydrological

116 years. Contrasting exposure to wind is considered in our analysis, and we test the
117 following hypotheses: 1) The proximity and the extent of open water areas close to
118 flooded forest sites will lead to different CO₂ fluxes in the forests. 2) Wind protected
119 forests will have lower *k* values and consequently lower CO₂ fluxes than wind exposed
120 sites. 3) Flooded forests have high rates of CO₂ evasion to the atmosphere and make a
121 large contribution to regional CO₂ evasion in the Amazon basin.

122

123 **2. Methods**

124 **2.1 Site description and sampling**

125 Measurements over two years were made in two contrasting flooded forest sites in
126 Lake Janauacá (3°23' S, 60°18' W; altitude 32 m), located on the southern side of the
127 Solimões River in the central Amazon basin (Figure 1). The sites differed in wind
128 exposure and fetch of adjacent open water areas and are called wind-exposed flooded
129 forest (WE) (3°23'19.0"S 60°15'14.8"W) and wind-protected flooded forest (WP)
130 (3°24'20.6"S 60°14'48.8"W). The WP site is in an embayment with a fetch of 50 to 100
131 m for typical wind directions. The WE site is located on the edge of the main lake and
132 had a fetch varying from 1 to 4 km depending on wind direction and water level.

133 The forests investigated are influenced by sediment and nutrient-rich water from
134 the Solimões River and are called *várzea* forests (Wittmann et al., 2002). Trees on
135 these floodplains respond phenologically, morphologically and physiologically to
136 periodic flooding, that varies as a function of the water level of the Solimões River and
137 the topography of the aquatic terrestrial transition zone (ATTZ) (Worbes 1997; Parolin et
138 al., 2010). Phenological behavior is largely associated with the time and extent of

139 inundation, and evergreen, semi-deciduous and deciduous species shred their leaves at
140 different times (Parolin et al., 2010). *Piranhea trifoliata* and *Vitex cymosa* are common
141 tree species (Worbes et al., 1992). The Janauacá floodplain and nearby systems have
142 been the focus of prior studies of hydrology and limnology (Melack & Forsberg 2001;
143 Melack et al., 2009; Bonnet et al. 2017).

144 Measurements of carbon dioxide partial pressure ($p\text{CO}_2$) and CO_2 emissions
145 were made when the sites were flooded and accessible at multiple times of the day and
146 night. Measurements were made on 12 occasions between August 2014 and
147 September 2016, representing different hydrological phases. The following periods were
148 sampled: August 2014 (falling water - FW), February to April 2015 (rising water - RW),
149 May to July 2015 (high water -HW), August 2015 (FW), September 2015 (FW), July
150 2016 (HW), and August and September 2016 (FW). The WP site was sampled in all
151 campaigns, while the WE site only in 2015 (Figure S1).

152 **2.2 - Analytical methods**

153 $p\text{CO}_2$ was measured with an off-axis integrated cavity output spectrometer
154 (Ultraportable Greenhouse Gas Analyzer (UGGA), Los Gatos Research) connected to a
155 marble-type equilibrator (Frankignoulle et al., 2001), through which water from different
156 depths was pumped (3 L min^{-1}). CO_2 fluxes across the air-water interface were
157 measured using floating chambers connected in a closed loop to the UGGA. All
158 measurements were made in replicate as ~10-minute deployments from a moored boat.
159 The chambers had an internal volume of 15 L and an internal area of 0.11 m^2 . Fluxes
160 were calculated from the slope of partial pressure versus time which was linear with r^2
161 greater than 0.9. The detection limit of our fluxes measurements was calculated as 0.22

162 mmol m⁻² h⁻¹ of CO₂. Further details of the equilibrator setup and gas analyzer accuracy
163 are given in Amaral et al. (2018), and for the chamber design in Barbosa et al. (2016).

164 We estimated gas transfer velocity (k) from the formulation $F = k[\Delta\text{CO}_2]$ using
165 our measurements of CO₂ fluxes (F) and the difference between observed and
166 equilibrium gas concentrations (ΔCO_2) derived from the $p\text{CO}_2$ measurements in water
167 and air and using Henry's constant. To estimate the gas concentrations in water and air,
168 we first corrected the dry air in the instrument to wet air using the water vapor computed
169 from temperature measured at lake surface (Weiss & Price, 1980), and then used the
170 Henry's constant for CO₂ from Wiesenburg & Guinasso (1979) to calculate
171 concentration. Estimated k values were normalized to 20°C (k_{600}) for which 600 is the
172 Schmidt number for CO₂ at 20°C and Sc at other temperatures were obtained from
173 Wanninkhof (1992).

174 Surface pH (Orion Star, Thermo Scientific; precision of 0.1, calibrated with 4.0
175 and 7.0 standards), maximum depth measured with a weighted graduated line, and
176 depth profiles of conductivity and temperature measured with a profiler (Castway,
177 Sontek Inst. Co) at 0.3 m intervals were obtained during each sampling period. Time
178 series measurements of temperature and dissolved oxygen (DO) were obtained at each
179 site using thermistors with 0.002°C accuracy (RBRsolo) recording every 0.5 s, and with
180 optical dissolved oxygen sensors (PME MiniDOT loggers) recording every 10 minutes
181 (accuracy of 5% of measurement or 0.3 mg L⁻¹, whichever is larger, and resolution of
182 0.01 mg L⁻¹). Wind speed and direction sensors (Onset, Inc.) were deployed at a height
183 of 2 m on a floating buoy at open water sites close to flooded forest sites. Average wind
184 speeds were calculated for the hour before the flux measurements.

185 Samples from ~0.3 m for chlorophyll (Chl-*a*), dissolved organic carbon (DOC),
186 total suspended solids (TSS), total nitrogen (TN) and total phosphorus (TP) analyses
187 were collected once on each campaign at both stations. Chl-*a* samples were filtered
188 through glass fiber GF/F filters (Whatman) and kept frozen in the dark until analysis.
189 Chl-*a* was determined spectrophotometrically, following filter maceration and extraction
190 in 90% acetone, using the trichromatic equations of Strickland & Parsons (1972). TSS
191 was determined by weighing particulates collected on pre-weighed Millipore HA filters
192 (0.45 µm pore size), following the method of Kasper et al. (2018). DOC samples were
193 filtered through pre-combusted (450–500°C for 1 h) glass fiber GF/F filters (Whatman),
194 collected in pre-cleaned (10% HCl wash, deionized water rinse) and pre-combusted
195 (450–500°C for 1 h) borosilicate vials and then stored at 4°C until analysis. DOC was
196 determined using a total organic carbon analyzer (TOC-V Shimadzu). TN and TP were
197 determined by simultaneous analysis on unfiltered samples after persulfate digestion
198 (Valderrama, 1981) followed by nitrate and phosphorus assays (Strickland & Parsons,
199 1972).

200 We estimated flooded forest area for the northern portion of Janauacá for each
201 sampling date using an image classification method to discriminate floodable forest
202 habitats and other land covers and a digital elevation model (DEM) derived for the lake
203 (Pinel et al., 2015). Forest vegetation (including trees and shrubs) was classified using
204 all bands of a Landsat 8 OLI image acquired in April 2016, when all floodable shrubs
205 and trees were emergent. We used eCognition software to perform multi-resolution
206 image segmentation, delineating homogeneous land cover units within the image. We
207 then developed classification rules to discriminate forest and shrub areas based on the

208 Normalized Difference Vegetation Index and the Normalized Difference Water Index
209 (Gao, 1996). We used the DEM and daily observations of water surface elevation, made
210 at a differential GPS calibrated gauging station on the lake (Pinel et al., 2015), to
211 estimate inundated area for each sampling occasion. Finally, we used the classified
212 image together with the inundation maps to estimate the total area of flooded forest for
213 each sampling period.

214 To account for the influence of forests with different wind exposure on CO₂
215 fluxes, we separated the flooded forest into two categories: 1) sheltered flooded forest
216 (WP), representative of flooded forests at the WP site, and 2) wind-exposed flooded
217 forest (WE), similar to that found at the WE site. To define the WE forest area we
218 delimited the perimeter of the largest open water area in the lake and then selected a
219 100 m band of forest immediately adjacent to this region. All remaining flooded forest
220 was defined as WP. All analyses were done with ArcGIS version 11.0 (ESRI, Inc.).

221 To combine measurements of fluxes and estimates inundated forest areas to
222 calculate annual fluxes (F , Gg C y⁻¹) from the flooded forests in the northern region of
223 Janauacá an expression similar to that in Melack et al. (2004) was used:

$$224 \quad F = \sum_{j=1}^2 \sum_{i=1}^8 (f_{ij} \cdot A_{ij} \cdot t)$$

225 f is the mean daily flux of CO₂ for each month and site (g C m⁻² d⁻¹), A is flooded forest
226 area for each month (km²), t is the number of days per month, i is the index for each
227 month (from February to September), and j is the index for each site (WP and WE).

228 To estimate the uncertainty of the estimates we conducted a Monte Carlo error
229 analysis using the measurements obtained each month and for data lumped into RW,
230 HW and FW periods. To do so, we randomly re-sampled with repetition the

231 measurements for each period to create 100 artificial data and computed the arithmetic
232 mean (m) and standard deviation (std) of these data using the *bootstrap* function in
233 Matlab. We then computed the maximum likelihood estimators as $MLE = \exp(m + std$
234 $^2/2)$ and 95% confidence intervals, CI (Dixon, 1993).

235

236 **2.3- Statistical Analyses**

237 CO_2 concentration, k_{600} , and CO_2 fluxes were compared between WP and WE
238 sites for only the first year as WE sites were not accessible in the second year. Tests for
239 normality and homoscedasticity indicated that CO_2 concentrations were normally
240 distributed, but k_{600} and CO_2 fluxes were not unless log transformed. Parametric tests
241 were used in all comparisons, using log transformed data, as required. The student t-
242 test was used for comparisons between WP and WE sites. A one-way ANOVA followed
243 by post-hoc pair-wise t-tests, with correction for multiple tests done by the Benjamin-
244 Hochberg method, was used to compare hydrological periods. We separated
245 measurements conducted over 24 h into categories of day (6:00 am to 6:00 pm) and
246 night (6:00 pm to 6:00 am) to evaluate the implications of sampling time for CO_2 fluxes,
247 variability of k_{600} , and CO_2 concentrations. We compared day and night values using all
248 data and data separated by site by paired t-test.

249 To assess the potential influences of environmental variables on CO_2
250 concentrations measured in flooded forests with contrasting wind exposure, we applied
251 a multi-model selection and averaging approach (Grueber et al., 2011) of linear mixed-
252 effects models with maximum likelihood using the *lme4* package in R. The model was
253 structured with CO_2 concentration as a response variable, site (WP and WE) as random

254 factors, and the total area of flooded forest for each sampling period, surface
255 temperature, TSS, DO, TN, TP, DOC, and Chl-a as fixed variables. We generated and
256 evaluated the small-sample corrected Akaike information criterion (AICc), Δ AICc, and
257 AICc model weights (w_i) using the *dredge* function within the *MuMIn* package (Barton &
258 Barton, 2018). The final model sets were simplified from all possible models by retaining
259 only the top models within two units of Δ AICc of the 'best' model. We calculated a daily
260 geometric mean of CO₂ concentration for each site and sampling occasion, and used
261 these values in the models, as we made only one measurement in each campaign for
262 some environmental predictors: Chl-a, TP, TN, DOC, TSS. Before model selection, we
263 first tested for outliers among explanatory variables (one exclusion was made). Second,
264 we identified and excluded from the full model co-linear predictors. For these steps, we
265 use the outlierTest and vif function respectively, both within the package car (Fox et al.,
266 2012).

267 To estimate parameter coefficients in the final model set, we calculated conditional
268 values using the mean of regression coefficients weighted by the AICc weight (w_i) from
269 each model including that variable (Burnham & Anderson, 2002). Predictor relative
270 importance, or variable weights, were calculated for each term in the models via the
271 natural average method for the coefficients, i.e., by summing the weights of models
272 where each variable appears (Grueber et al., 2011, Galipaud et al., 2014). Using z-
273 tests, individual parameters in model-averaged sets were tested for statistical
274 significance as the deviation of coefficients from zero. Parametric assumptions of linear
275 models were verified using plots of residuals for normality and homoscedasticity.
276 Statistical analyses and graphics were done with R Studio Version 1.1.456.

277 **3. Results**

278 **3.1 - CO₂ concentrations and fluxes**

279 Surface CO₂ concentrations ranged from 19 to 329 μM (*p*CO₂ = 664 to 11006 μatm);
280 the overall geometric mean was 134 μM, and the mean and standard deviation were
281 155 ± 71 μM (*p*CO₂ = 4465; 5117 ± 2326 μatm) (Table 1). 170 measurements of CO₂
282 flux were made at the two flooded forests sites, and fluxes ranged from -0.8 to 55 mmol
283 m⁻² h⁻¹ with an overall mean and standard deviation of 7.8 ± 10.1 mmol m⁻² h⁻¹ (Table 1).
284 Gas transfer velocities derived from these measurements ranged from 0.2 to 17 cm h⁻¹
285 with an overall geometric mean value of 2.6 cm h⁻¹ and mean and standard deviation of
286 3.8 ± 3.6 cm h⁻¹ (Table 1). Mean CO₂ concentrations were similar at the two sites (WE,
287 175 ± 65 μM and WP, 178 ± 60 μM; Welch two sample t-test, $t(58) = 0.2$, $p=0.84$) (Figure
288 2). CO₂ fluxes and *k*₆₀₀ were greater at the WE site (16 ± 14 mmol m⁻² h⁻¹ and 6.7 ± 4.6
289 cm h⁻¹) compared to the WP site (5 ± 3 mmol m⁻² h⁻¹ and 2.4 ± 1.7 cm h⁻¹) based on
290 Welch two sample t-test ($t(82)=-5.4$, $p<0.001$ and $t(112.2)=-7.9$, $p<0.001$, respectively).

291 Surface CO₂ concentrations differed seasonally at the WE site based on one-way
292 ANOVA ($F(2,24)=4.9$, $p=0.02$). Values were higher during high water (HW) (218 ± 36
293 μM, $n=19$) relative to rising water (RW) (143 ± 89 μM, $n=14$), but similar (pairwise t test,
294 $p=0.14$) to concentrations during falling water (FW) (173 ± 39 μM, $n=25$) (Figure 2).
295 Seasonal differences also occurred at the WP site ($F(4,48)=9.9$, $p<0.001$). In year one,
296 the CO₂ concentrations measured at the WP site were higher during HW (203 ± 20 μM,
297 $n=18$) and FW (193 ± 71 μM, $n=32$) compared to RW (154 ± 47 μM, $n=20$) (pairwise t-
298 test, $p=0.03$ and $p=0.05$, respectively). In year two, no differences were found between

299 HW ($81 \pm 38 \mu\text{M}$, $n=21$) and FW ($96 \pm 64 \mu\text{M}$, $n=21$), but mean surface CO_2
300 concentrations measured in those periods were consistently lower than the values
301 measured in HW and FW periods of the first year of study (pairwise t-test, $p<0.001$)
302 (Table 1).

303 CO_2 fluxes and k_{600} for both sites varied with the phase of the hydrological cycle
304 based on one-way ANOVA. At the WE site, CO_2 fluxes ($F(2,55)=19$, $p<0.001$) and
305 values of k_{600} ($F(2,55)=17$, $p<0.001$) tracked changes in the water level, with greater
306 mean values observed during high water ($29 \pm 14 \text{ mmol m}^{-2} \text{ h}^{-1}$ and $11 \pm 4 \text{ cm h}^{-1}$, $n=19$)
307 relative to rising ($9 \pm 8 \text{ mmol m}^{-2} \text{ h}^{-1}$ and $5 \pm 2 \text{ cm h}^{-1}$, $n=14$) and falling water (9 ± 7
308 $\text{mmol m}^{-2} \text{ h}^{-1}$ and $5 \pm 4 \text{ cm h}^{-1}$, $n=25$) (Pairwise t-test, $p<0.001$)(Figure 3). At the WP
309 site, mean CO_2 fluxes ($F(4,107)=16.2$, $p<0.001$) were also higher during high water (6 ± 3
310 $\text{mmol m}^{-2} \text{ h}^{-1}$, $n=18$) compared to falling water ($4 \pm 2 \text{ mmol m}^{-2} \text{ h}^{-1}$, $n=32$), but similar to
311 mean values encountered during rising water ($6 \pm 4 \text{ mmol m}^{-2} \text{ h}^{-1}$, $n=20$) of year one
312 (Pairwise t-test, $p=0.001$)(Figure 3). Differences in mean k_{600} between periods of the
313 hydrological cycle ($F(4,107)=4.6$, $p=0.002$) were higher when comparing the rising water
314 ($3 \pm 2 \text{ cm h}^{-1}$, $n=20$) and high water periods ($3 \pm 1 \text{ cm h}^{-1}$, $n=18$) against the falling water
315 period ($2 \pm 1 \text{ cm h}^{-1}$, $n=32$) in year one (Pairwise t-test, $p=0.01$ and $p=0.02$,
316 respectively). In year two, mean CO_2 fluxes for a given period of the hydrological cycle
317 were consistently lower than the mean values measured in all periods of year one at the
318 WP site (pairwise t-test, $p<0.001$) (Table 1). For k_{600} the falling water period of year two
319 was similar to the falling water period of year one (pairwise t-test, $p=0.99$), and also
320 lower than high water (pairwise t-test, $p=0.03$) and rising water periods (pairwise t-test,
321 $p=0.02$) of year one (Table 1).

322 Day-night differences were statistically different for CO₂ fluxes when comparing
323 all measurements at both sites (Paired t-test, t(11)= 3.8, p=0.003). When differentiating
324 between WP and WE sites, mean CO₂ concentrations were numerically lower during the
325 day (WP=128 ± 68 μM, n=33, and WE=166 ± 56 μM, n=13) compared to the night
326 (WP=172 ± 72 μM, n=20, and WE=183 ± 74 μM, n=14) at both sites, although they
327 were not statistically different (Paired t-test, WP: t(11)= -0.63, p=0.54; WE: t(7)= -0.4,
328 p=0.74). CO₂ fluxes and *k*₆₀₀ were statistically different only for the WP site. CO₂ fluxes
329 (Paired t-test, t(11)= 2.7, p=0.02) and *k*₆₀₀ (Paired t-test, t(11)= 2.7, p=0.02) were lower
330 during the night (3.6 ± 2.6 mmol m⁻² h⁻¹ and 2 ± 0.5 cm h⁻¹, n=42) compared to the day
331 (3.9 ± 3.3 mmol m⁻² h⁻¹ and 3 ± 2 cm h⁻¹, n=70) (Figure 4), and consistent with day-night
332 differences at this site for wind speeds that were also higher during the day compared to
333 the night (Unpaired t-test, t(51) = 3.5 , p=0.0009). Although not significantly different, we
334 found numerically higher mean values for CO₂ fluxes and *k*₆₀₀ during the night (20 ± 17
335 mmol m⁻² h⁻¹ and 8 ± 5 cm h⁻¹, n=29) compared to the day (12 ± 9 mmol m⁻² h⁻¹ and 6 ±
336 4 cm h⁻¹, n=29) at the WE site. Wind differences at this site followed the same trend as
337 for the WP site with higher wind speeds during the day (Unpaired t-test, t(24) = 2.2 ,
338 p=0.04) but the higher fluxes during the night were associated with vertical mixing
339 (Figure 5).

340 **3.2 - Environmental variables and relationships with CO₂ concentrations**

341 Environmental variables varied with water level. When depths were low during
342 rising and falling water, Chl-a, DO, TN, TSS, conductivity and temperatures were higher
343 compared to high water. Average hourly wind records prior to CO₂ flux measurements
344 varied from below detection to 2.2 m s⁻¹ at the WP site and from 0.3 to 5.1 m s⁻¹ at the

345 WE site (frequency distributions are given in Figure S2). Environmental variables for
346 both sites are summarized in supporting information (Table S1).

347 DO was strongly inversely correlated to CO₂ concentrations (n=80, r²= -0.86,
348 p<0.001). We identified one outlier among our environmental variables. The outlier was
349 high chlorophyll and high CO₂ concentrations that occurred at the WP site during the
350 falling water in 2015. At that time, the thermocline deepened causing upwelling of
351 nutrient-enriched waters that caused an increase in chlorophyll, and water enriched in
352 CO₂ concentration was upwelled that raised CO₂ concentrations. DO was the only
353 environmental predictor that was retained from the multi-model selection procedure. It
354 has an AICc value of 149.9 and explained around 90% (marginal R²) or 97%
355 (conditional R²) variability in surface CO₂ concentration.

356 **3.3 - Spatial and seasonal integration of CO₂ fluxes**

358 The WP forests in the northern Janauacá floodplain had a total area of 94 km²,
359 which corresponds to 88% of the total area of floodable forest estimated for this part of
360 the lake. The remaining 12% is attributed to areas with WE forests.

361 The maximum likelihood estimator of the flux for all inundated forests in the
362 Janauacá floodplain is 45 Gg C y⁻¹ with CI of 31 to 69 Gg C y⁻¹. Emissions from
363 sheltered forests represent 31 Gg C y⁻¹ with CI of 21 to 49 Gg C y⁻¹ and those from wind
364 exposed forests 14 Gg C y⁻¹ with CI of 10 to 20 Gg C y⁻¹. These values were almost the
365 same based on calculations per month and for data lumped into hydrological periods.

366 We obtained a regional estimate based on the area of flooded vegetation and
367 open water during high and low water for a sequence of reaches along the Solimões
368 and Amazon rivers in the central Amazon basin using data in Melack & Hess (2010).

369 From Marañón to Gurupá their high water area of flooded forests, woodlands and
370 shrubs (52,700 km²) combined with our high water estimates of CO₂ flux, using the
371 proportional areas of wind-sheltered and wind-exposed forest calculated for Janauacá,
372 yields a total high water flux of 133 ± 65 Tg C for these reaches. When extrapolated to
373 the total high water area of flooded forests, woodlands and shrubs for the lowland basin
374 (630,000 km²) (Melack & Hess 2010), the total high water flux is 1,590 ± 780 Tg C.

375

376 **4. Discussion**

377 **4.1 - Diel, seasonal and spatial variability of CO₂ concentrations and fluxes**

378 As we hypothesized, the WE site near a large area of open water had higher CO₂
379 fluxes and *k* values compared to the more sheltered WP site. This result is related to the
380 increased advection, mixing and turbulence occurring in sites near large open water
381 areas. Daily fluxes measured in our study are higher than or similar to the few other
382 measurements in waters within tropical and subtropical flooded forests (Table 2). This
383 finding supports our suggestion that flooded forests have high rates of CO₂ evasion to
384 the atmosphere and make a large contribution to regional CO₂ evasion in the Amazon
385 basin.

386 While our time series data supports previous studies that CO₂ concentrations and
387 fluxes vary seasonally, the frequency of our measurements further illustrated that
388 variability was high at each site and during each measurement period. We corroborate
389 previous studies reporting higher CO₂ concentrations and fluxes during the high water
390 period for Amazonian rivers (Richey et al., 1990; Devol et al., 1995; Almeida et al. 2017;
391 Amaral et al., 2019) and floodplain lakes (Rudorff et al., 2011; Abril et al., 2014). The

392 seasonal pattern can be explained by (i) increases in water depth that increase depth
393 integrated respiration (Devol et al., 1995; Forsberg et al., 2017), and (ii) the extent of
394 inundation of the floodplains. CO₂ concentrations in floodplains are positively related to
395 the area of inundated vegetated habitats (Abril et al., 2014; Borges et al., 2015; Amaral
396 et al., 2019), that are greater during the high water period (Melack & Hess, 2010). The
397 vegetated habitats contribute particulate organic carbon and DOC to the floodplains that
398 can be decomposed in situ, generating CO₂ and CH₄, buried in the sediments, or
399 transported laterally to the rivers (Richey et al., 1988;1990; Melack & Forsberg, 2001;
400 Engle et al., 2008; Melack & Engle, 2009). Additionally, they contribute CO₂ to
401 floodplain waters via root respiration (Hamilton et al., 1995; Piedade et al., 2010a).

402 Day-night differences were one source of the variability but were statistically
403 significant only for CO₂ fluxes and k_{600} at the WP site with higher mean values during
404 the day. Wind-induced currents or internal waves within the stratified waters of the
405 flooded forests and neighboring habitats may have transported or mixed water with
406 elevated CO₂ concentrations into the surface waters within the flooded forest. Near-
407 surface turbulence in the forest may have increased in the day due to advective flows
408 generated outside the forest and higher wind speeds resulting in higher gas transfer
409 velocities (MacIntyre et al., 2019). Values of k_{600} under these conditions will be higher
410 than those expected from convection at night when winds are negligible. At the WE site,
411 values were similar during the day and night except on two occasions when fluxes at
412 night were nearly twice those in the day (Figure 4A). These occurred during high water
413 in May and June 2015 when water depths were 5 to 7 m, depths where CO₂ did
414 accumulate, and anoxia developed because stratification can persist. The actively

415 mixing layer increased from 1.2 m to 6 m at night, as indicative of mixing, and surface
416 CO₂ concentrations increased (Figure 5). Fluxes increased as a result.

417 The variability of k_{600} was higher at the WE site as were mean values (6.7 ± 4.6
418 SD) relative to the WP site (2.3 ± 1.6 SD) (Figure S3). The higher k_{600} values are likely
419 associated with increases in shear in the surface waters of the flooded forest caused by
420 wind-induced water currents from nearby open water (MacIntyre et al., 2019). Ho et al.
421 (2018) obtained similar results in the Everglades.

422 Between year variability in surface water CO₂ concentrations occurred at the WP
423 site. Values were higher in year 1, likely because of more extensive and a longer
424 inundation. Additionally, floating macrophytes whose decay and root respiration
425 contributes to CO₂ in the water column (Waichman, 1996; Mortillaro et al., 2016;
426 Hamilton et al., 1995) were present in year 1 but not in year 2. Advective flows can
427 transport this water with higher gas concentration into the flooded forests. Thus,
428 between year differences in the hydrological conditions contribute to variability.

429 The interannual differences have implications for understanding possible impacts
430 of climate change in tropical floodplains. For example, extreme events are increasing in
431 frequency in the Amazon basin (Marengo & Espinoza, 2016), and projected climate
432 change scenarios indicate reductions in the extent of inundated areas during the low
433 water period (Sorribas et al., 2016), similar to our observations in year 2. Our results
434 support a reduction in CO₂ concentrations and fluxes from flooded forests under this
435 scenario. However, we did not measure the fluxes from exposed sediments. Evidence
436 from other studies in flooded forests in tropical (Tathy et al., 1992) and temperate
437 (Pulliam, 1993; Happell & Chanton, 1993) zones report positive CO₂ fluxes from non-

438 flooded sediments in the floodable forest. However, Dalmagro et al. (2019) reported
439 CO₂ fluxes in-gassing during flooded season and outgassing during dry season in a
440 study in seasonally inundated forests of the Pantanal floodplain. Additional
441 measurements from exposed sediments during the non-inundated phase are needed to
442 allow a better evaluation of the impacts of variations in inundation periods.

443 **4.2- Inverse relation between CO₂ concentrations and dissolved oxygen**

444 An inverse relation between CO₂ concentrations and dissolved oxygen was
445 observed in this study as in many freshwater ecosystems, including tropical floodplains
446 along sub-Saharan African rivers (Borges et al., 2015), the Pantanal (Hamilton et al.,
447 1995), and temperate swamp forests (Happell & Chanton 1993). In the Pantanal
448 wetlands, the highest CO₂ concentrations and fluxes occurred as flooding began
449 because of decomposition of freshly inundated soil and plant organic matter (Hamilton
450 et al., 1997; Dalmagro et al., 2018). The inverse relation between CO₂ concentrations
451 and dissolved oxygen suggests that aerobic processes are important for CO₂
452 production. Sediment respiration (Cardoso et al., 2013), methane oxidation (Barbosa et
453 al., 2018), and planktonic respiration (Waichman, 1996; Ward et al., 2013; Amaral et al.,
454 2018) are all processes that consume dissolved oxygen and produce dissolved CO₂.

455 More CO₂ was produced at our sites than expected by aerobic respiration within
456 the water column (Figure 6). If aerobic respiration and CO₂ production were in balance,
457 the excess of CO₂ (Ex-CO₂, i.e., CO₂ in the water subtracted from equilibrium CO₂
458 saturation) and the apparent oxygen utilization (AOU, i.e., atmospheric equilibrium O₂
459 solubility subtracted from the O₂ concentration measured in surface water) would follow
460 a 1:1 line. Processes that could cause increased CO₂ production or elevated Ex-CO₂

461 include methanogenesis (Bartlett et al., 1988), groundwater CO₂ inputs, and root
462 respiration within the flooded forest and associated herbaceous plants that use
463 atmospheric CO₂ in photosynthesis and release respired CO₂ through their inundated
464 roots (Melack et al., 2009; Piedade et al., 2010b; Abril et al., 2014; Abril & Borges,
465 2019). The first two processes were not likely to be important at our sites. Ex-CO₂ was
466 not correlated with methane measured at these sites (Barbosa, 2018) ($p > 0.05$,
467 $r^2 = 0.0063$ slope = 0.0019), and the contribution of groundwater to the hydrologic
468 balance is less than 1% in Janauacá (Bonnet et al., 2017).

469 The Ex-CO₂ vs AOU relation in our study is similar to the relation reported for the
470 Solimões River and other Amazon waters (Devol et al., 1995; Richey et al., 1988).
471 These studies suggested the importance of lateral floodplains as sites for CO₂
472 production and sources to the rivers. This hypothesis was examined by Abril et al.
473 (2014), who used a one-dimensional model for CO₂ transport by the Amazon River to
474 demonstrate that CO₂ from floodplains could be transported downstream over hundreds
475 of kilometers. Further evidence of inputs of labile organic carbon to the rivers from
476 floodplains is provided by measurements in the eastern Amazon by Moreira-Turcq et al.
477 (2013). Moreover, Richey et al. (1990) suggested that aquatic and terrestrial
478 macrophytes and flooded forests in floodplains were likely sources of labile organic C
479 for the mainstem river.

480 We also observed negative AOU values that represent times when
481 photosynthetic oxygen production exceeded respiration within the flooded forests. The
482 negative AOU values occurred when water depths were 1.5 to 3.5 m and DO

483 concentrations were 7.4 to 9.3 mg L⁻¹ in the flooded forest sites. These concentrations
484 were similar to those observed in nearby open water.

485 **4.3 Implications for the regional C budget and other forested wetlands**

486 To our knowledge, we provide the first multi-season study of CO₂ concentrations
487 and fluxes in flooded forests for the Amazon basin. The one prior study reported nine
488 CO₂ measurements made in July and August 1985 in flooded forests fringing open
489 water areas, similar to our WE site (Devol et al., 1988). The range of values in that
490 study, 466 - 2400 mg C m⁻² d⁻¹, is lower than the range, 3706 - 15867 mg C m⁻² d⁻¹,
491 (n=19) observed during a comparable period of our study, high water at the WE site.

492 Mean daily fluxes measured in our study (2182 ± 2954 SD mg C m⁻² d⁻¹) are
493 higher than or similar to the few other measurements in waters within tropical and
494 subtropical flooded forests (Table 2). The low CO₂ efflux reported by Dalmagro et al.
495 (2018) is likely related to their use of a wind-based equation to estimate the CO₂ fluxes.
496 While wind speeds in flooded forest sites are low, other processes can increase fluxes,
497 as noted above and in MacIntyre et al. (2019). The large range in our study indicates
498 the need for a sampling over diel cycles on a seasonal basis (Table 2).

499 Seasonally inundated and riparian forests are the main aquatic habitat within the
500 lowland Amazon basin (Junk et al., 2010; Melack & Hess, 2010; Hess et al., 2015).
501 Most of these forests are likely to be more similar to our WP site, as the open water
502 areas in the lowland Amazon basin corresponds to only 8% of the total basin area
503 (Melack & Hess 2010). Inundated forests vary in distribution and floristic composition
504 depending on fluvial geomorphology, flooding regimes, and soil and water qualities
505 (Junk et al. 2010). CO₂ fluxes among these forest types are likely to vary.

506 We report a total high water flux, integrated to the area of flooded forests,
507 woodlands and shrubs during this period, for the lowland Amazon of $1,590 \pm 777$ Tg C.
508 For comparison, Melack & Hess's (2010) estimate of open water in rivers and lakes at
509 high water ($64,700 \text{ km}^2$) and the mean CO_2 fluxes reported mainly for rivers by Amaral
510 et al. (2019; $4.7 \text{ g C m}^{-2} \text{ d}^{-1}$) and Richey et al. (1990; $5.2 \text{ g C m}^{-2} \text{ d}^{-1}$) yields a total high
511 water flux from open water of 320 Tg C. Since fluxes from lakes are often less than from
512 rivers (Rudorff et al., 2011; Polsenaere et al., 2013; Melack, 2016), this estimate for
513 open water is likely high. At low water, Melack & Hess (2010) estimated that flooded
514 forests, woodlands and shrubs covered $17,270 \text{ km}^2$ of the mainstem reaches. To
515 provide annual estimates will require time series of inundated habitats derived from
516 hydrological models and remote sensing analysis, such as those done by Arnesen et al.
517 (2013) and Ferreira-Ferreira et al. (2015), that map the duration of inundation of flooded
518 forests distributed throughout the Amazon basin. Measurements of CO_2 fluxes from
519 other types of flooded forests are also essential.

520 Regional estimates of CO_2 fluxes offered by Richey et al. (2002) and Melack
521 (2016) did not include data from flooded forests. Melack's (2016) estimate for
522 floodplains and wetland habitats used an average $p\text{CO}_2$ value ($335 \text{ }\mu\text{M}$; $10900 \text{ }\mu\text{atm}$)
523 from Richey et al. (2002) and k_{600} of 12 cm h^{-1} from studies in lakes. Our lower k_{600}
524 values for flooded forests, a large component of floodplain and wetland habitats, clearly
525 indicates a lower overall flux than suggested in Melack (2016). Richey et al. (2002)
526 selected a k_{600} of 2.7 cm h^{-1} as a conservative value for floodplains and lakes. Though
527 low for lakes, this value is similar to our k_{600} values for sheltered flooded forests. As a
528 consequence, their regional estimate, if expressed as $\text{mmol C m}^{-2} \text{ d}^{-1}$ (189 ± 55) is

529 similar to our mean value (182 ± 247) for flooded forests on the Janauacá floodplain.

530 These new estimates highlight the importance of flooded forests for the carbon budget
531 of the Amazon basin and the need for more studies in these aquatic habitats.

532 Seasonally inundated forests in the Amazon and elsewhere occur in an aquatic-
533 terrestrial transition zone that includes other aquatic habitats such as open waters and
534 macrophytes. Integration of C fluxes in the ATTZ is challenging, as the aquatic habitats
535 are interconnected and interact with each other. For comparison, we contrast our mean
536 CO₂ evasion with an estimate of net primary production (NPP) of 1150 Mg C km⁻²y⁻¹ for
537 flooded forests in the central Amazon basin (Worbes 1997; Melack & Forsberg 2001).
538 This rate is based on 30% of the live wood increment, fine litter, and large woody
539 detritus inputs to the aquatic system. Our mean CO₂ evasion (590 MgC km⁻²y⁻¹) is about
540 half of the NPP estimate, considering that these forests remain flooded for 270 days a
541 year. The excess of C inputs from NPP corroborates findings by other studies that
542 argue for the mixed C sources to supply CO₂ evasion rates in open waters of the
543 Amazon basin (Quay et al., 1992; Melack & Forsberg 2001; Engle et al., 2008; Ward et
544 al., 2013; 2016).

545 We suggest that C studies in aquatic habitats of ATTZ integrate C fluxes by
546 weighting their relative areal coverage in the floodplain. This practice will avoid over-
547 representation of recent floodplain CO₂ flux estimates (e.g., Rasera et al., 2013; Melack,
548 2016) that are based mainly on data obtained from open water habitats, but
549 extrapolated to areas that encompass other aquatic habitats with different
550 characteristics and typically lower emissions, such as flooded forests and floating

551 macrophytes. Future studies in flooded forests should aim to improve estimates of tree
552 stem CO₂ fluxes as well as fluxes from soil when these forests are not inundated.

553 Abril & Borges (2019) review the conceptual framework of carbon fluxes in the
554 terrestrial aquatic continuum and highlight the need for including flooded land as a
555 component in this continuum. They propose that C fluxes from flooded lands should be
556 treated as a transport term between upland and inland waters. An example of their
557 conceptual framework is provided by an organic carbon budget developed by Melack &
558 Engle (2009) for an Amazon floodplain lake. More C budgets studies in flooded lands
559 are needed as the basis for modeling studies as well as to provide correct comparisons
560 between the terrestrial and aquatic C fluxes.

561 The results from our study demonstrate the importance of combining gas
562 measurements with meteorological and limnological information to understand CO₂
563 fluxes in flooded forests. Additional direct measurements of *k* and studies of the
564 mechanisms that generate turbulence and effects on *k*₆₀₀ under low wind speed
565 conditions are needed. We recommend that further studies include measurements
566 throughout the day and night. The contrasting *k* and CO₂ fluxes values observed in
567 sheltered flooded forests versus wind exposed forests should be considered in the
568 integration of CO₂ fluxes in forested wetlands.

569

570

571

572

573

574 **Acknowledgements**

575 This work was supported by the Conselho Nacional de Pesquisa e Desenvolvimento—
576 Ministério da Ciência Tecnologia (CNPq/MCTI); CNPq/LBA-Edital.68/2013, processo
577 458036/2013-7, CNPq-Universal processo.482004/2012-6. Post- graduate scholarships
578 were provided to JHFA and by Coordenação de Aperfeiçoamento de Pessoal de Nível
579 Superior (CAPES) and CNPq. PMB and JHFA are thankful to CAPES for the grant
580 “Programa de Doutorado Sanduíche no Exterior” - 88881.135203/2016-0100 and
581 88881.134945/2016-0100 respectively. During manuscript preparation support was
582 provided to JHFA and PMB by NASA grant NNX17AK49G. JMM received support from
583 National Aeronautics and Space Administration (NASA), the US Department of Energy
584 (Contract No. DE-0010620) and a Fulbright fellowship. The authors thank for the
585 logistical support of INPA, João B. Rocha for the field support, and Lúcia Silva for
586 offering the floating house as a research base. We thank Michaela Melo and Jonismar
587 S. da Silva for help in field campaigns, and Nicholas Marino for contributions regarding
588 statistical analyses and Alberto Vieira Borges for comments in an early version of the
589 manuscript.

590 Data statement: Data was deposited in the KNB data repository operated by NCEAS
591 and assigned a DOI: 10.5063/F1N8784V (<https://doi.org/10.5063/F1N8784V>.)

592 No authors have financial conflicts of interest.

593

594

595

596

597 **References**

598 Abril, G., & Borges, A. V. (2019). Ideas and perspectives: Carbon leaks from flooded
599 land: do we need to replumb the inland water active pipe? *Biogeosciences*, 16(3), 769–
600 784. <https://doi.org/10.5194/bg-16-769-2019>

601
602 Abril, G., Martinez, J.-M., Artigas, L. F., Moreira-Turcq, P., Benedetti, M. F., Vidal, L., et
603 al. (2014). Amazon River carbon dioxide outgassing fuelled by wetlands. *Nature*,
604 505(7483), 395–398. <https://doi.org/10.1038/nature12797>

605
606 Alin, S. R., Rasera, M. de F. F. L., Salimon, C. I., Richey, J. E., Holtgrieve, G. W.,
607 Krusche, A. V., & Snidvongs, A. (2011). Physical controls on carbon dioxide transfer
608 velocity and flux in low-gradient river systems and implications for regional carbon
609 budgets. *Journal of Geophysical Research*, 116 (G01009).
610 <https://doi.org/10.1029/2010JG001398>

611
612 Almeida, R. M., Pacheco, F. S., Barros, N., Rosi, E., & Roland, F. (2017). Extreme
613 floods increase CO₂ outgassing from a large Amazonian river. *Limnology and*
614 *Oceanography*, 62(3), 989–999. <https://doi.org/10.1002/lno.10480>

615
616 Amaral, J. H. F., Borges, A. V., Melack, J. M., Sarmiento, H., Barbosa, P. M., Kasper,
617 D., et al. (2018). Influence of plankton metabolism and mixing depth on CO₂ dynamics
618 in an Amazon floodplain lake. *Science of The Total Environment*, 630, 1381–1393.
619 <https://doi.org/10.1016/j.scitotenv.2018.02.331>

620

621 Amaral, J. H. F., Farjalla, V. F., Melack, J. M., Kasper, D., Scofield, V., Barbosa, P. M.,
622 & Forsberg, B. R. (2019). Seasonal and spatial variability of CO₂ in aquatic
623 environments of the central lowland Amazon basin. *Biogeochemistry*.
624 <https://doi.org/10.1007/s10533-019-00554-9>

625

626 Arnesen, A.S., Silva, T.S.F., Hess, L.L., Novo, E.M.L.M., Rudorff, C.M., Chapman, B.D.
627 & McDonald, K.C. (2013) Monitoring flood extent in the lower Amazon River floodplain
628 using ALOS/PALSAR ScanSAR images. *Remote Sensing of Environment* 130, 51–61.
629 <https://dx.doi.org/10.1016/j.rse.2012.10.035>

630

631 Barbosa, P. M., Farjalla, V. F., Melack, J. M., Amaral, J. H. F., da Silva, J. S., &
632 Forsberg, B. R. (2018). High rates of methane oxidation in an Amazon floodplain lake.
633 *Biogeochemistry*, 137(3), 351–365. <https://doi.org/10.1007/s10533-018-0425-2>

634

635 Barbosa, P. M. (2018). *Dinâmica do metano em um lago de planície de inundação*
636 *tropical* (Doctoral dissertation). Retrieved from [PPGEcologia UFRJ].
637 (<http://www.ppge.ufrj.br/teses>). Rio de Janeiro, RJ, Brazil: Universidade Federal do Rio
638 de Janeiro.

639

640 Bartlett, K. B., Crill, P. M., Sebacher, D. I., Harriss, R. C., Wilson, J. O., & Melack, J. M.
641 (1988). Methane flux from the central Amazonian floodplain. *Journal of Geophysical*
642 *Research*, 93(D2), 1571-1582. <https://doi.org/10.1029/JD093iD02p01571>

643

644 Bass, A., O'Grady, D., Leblanc, M., Tweed, S., Nelson, P., Bird, M. (2014) Carbon
645 dioxide and methane emissions from a wet/dry tropical floodplain in Northern Australia.
646 *Wetlands* 34(3), 619–627. <https://doi.org/10.1007/s13157-014-0522-5>

647

648 Barton, K., & Barton, M. K. (2018). Package 'MuMIn.' *Version*, 1, 18.

649

650 Borges, A. V., Darchambeau, F., Teodoru, C. R., Marwick, T. R., Tamooch, F., Geeraert,
651 N., et al. (2015). Globally significant greenhouse-gas emissions from African inland
652 waters. *Nature Geoscience*, 8(8), 637–642. <https://doi.org/10.1038/ngeo2486>

653

654 Bonnet, M. P., Pinel, S., Garnier, J., Bois, J., Resende Boaventura, G., Seyler, P., &
655 Motta Marques, D. (2017). Amazonian floodplain water balance based on modelling and
656 analyses of hydrologic and electrical conductivity data. *Hydrological Processes*, 31(9),
657 1702–1718. <https://doi.org/10.1002/hyp.11138>

658

659 Burnham, K. P. & Anderson, D. R. (2002). *Model selection and multimodel inference: a*
660 *practical information-theoretic approach* (2nd ed). New York: Springer.

661

662 Cardoso, S. J., Vidal, L. O., Mendonça, R. F., Tranvik, L. J., Sobek, S., & Fábio, R.
663 (2013). Spatial variation of sediment mineralization supports differential CO₂ emissions
664 from a tropical hydroelectric reservoir. *Frontiers in Microbiology*, 4.
665 <https://doi.org/10.3389/fmicb.2013.00101>

666

667 Cole, J. J., Prairie, Y. T., Caraco, N. F., McDowell, W. H., Tranvik, L. J., Striegl, R. G., et
668 al. (2007). Plumbing the global carbon cycle: Integrating inland waters into the terrestrial
669 carbon budget. *Ecosystems*, 10(1), 172–185. [https://doi.org/10.1007/s10021-006-9013-](https://doi.org/10.1007/s10021-006-9013-8)
670 [8](https://doi.org/10.1007/s10021-006-9013-8)

671

672 Dalmagro, H. J., Lathuillière, M. J., Hawthorne, I., Morais, D. D., Pinto Jr, O. B., Couto,
673 E. G., & Johnson, M. S. (2018). Carbon biogeochemistry of a flooded Pantanal forest
674 over three annual flood cycles. *Biogeochemistry*, 139(1), 1–18.
675 <https://doi.org/10.1007/s10533-018-0450-1>

676

677 Dalmagro, H. J., Zanella de Arruda, P. H., Vourlitis, G. L., Lathuillière, M. J., de S.
678 Nogueira, J., Couto, E. G., & Johnson, M. S. (2019). Radiative forcing of methane fluxes
679 offsets net carbon dioxide uptake for a tropical flooded forest. *Global Change Biology*,
680 25(6), 1967–1981. <https://doi.org/10.1111/gcb.14615>

681

682 Devol, A. H., Richey, J. E., Clark, W. A., King, S. L., & Martinelli, L. A. (1988). Methane
683 emissions to the troposphere from the Amazon floodplain. *Journal of Geophysical*
684 *Research*, 93(D2), 1583-1592. <https://doi.org/10.1029/JD093iD02p01583>

685

686 Devol, A. H., Forsberg, B. R., Richey, J. E., & Pimentel, T. P. (1995). Seasonal variation
687 in chemical distributions in the Amazon (Solimões) River: A multiyear time series.
688 *Global Biogeochemical Cycles*, 9(3), 307–328. <https://doi.org/10.1029/95GB01145>

689
690
691
692
693
694
695
696
697
698
699
700
701
702
703
704
705
706
707
708
709
710

Dixon, P. M. 1993. The bootstrap and the jackknife: Describing the precision of ecological indices, p. 290–318. In S.M. Scheiner and J. Gurevitch [eds.], *Design and analysis of ecological experiments*. Oxford University Press.

Engle, D.L., Melack, J.M., Doyle, R.D., & Fisher, T.R. (2008). High rates of net primary productivity and turnover for floating grasses on the Amazon floodplain: Implications for aquatic respiration and regional CO₂ flux. *Global Change Biology* 14, 369-381. <https://doi.org/10.1111/j.1365-2486.2007.01481.x>

Ferreira-Ferreira, J., Silva, T.S.F., Streher, A.S., Affonso, A.G, Furtado, L.F.A., Forsberg, B.R., Valsecchi, J., Queiroz, H.L., Novo, E.M.L.M. (2015). Combining ALOS/PALSAR derived vegetation structure and inundation patterns to characterize major vegetation types in the Mamirauá Sustainable Development Reserve, Central Amazon Floodplain, Brazil. *Wetlands Ecology and Management* 23, 41-59. <https://doi.org/10.1007/s11273-014-9359-1>

Forsberg, B. R., Melack, J. M., Richey, J. E., & Pimentel, T. P. (2017). Regional and seasonal variability in planktonic photosynthesis and planktonic community respiration in Amazon floodplain lakes. *Hydrobiologia*, 800(1), 187–206.

<https://doi.org/10.1007/s10750-017-3222-3>

711 Fox, J., Weisberg, S., Adler, D., Bates, D., Baud-Bovy, G., Ellison, S., et al. (2012).
712 Package 'car.' *Vienna: R Foundation for Statistical Computing*.

713

714 Frankignoulle, M., Borges, A., & Biondo, R. (2001). A new design of equilibrator to
715 monitor carbon dioxide in highly dynamic and turbid environments. *Water Research*,
716 35(5), 1344–1347. [https://doi.org/10.1016/S0043-1354\(00\)00369-9](https://doi.org/10.1016/S0043-1354(00)00369-9)

717

718 Galipaud, M., Gillingham, M. A. F., David, M., & Dechaume-Moncharmont, F.-X. (2014).
719 Ecologists overestimate the importance of predictor variables in model averaging: a
720 plea for cautious interpretations. *Methods in Ecology and Evolution*, 5(10), 983–991.
721 <https://doi.org/10.1111/2041-210X.12251>

722

723 Gao, B. (1996) NDWI—A normalized difference water index for remote sensing of
724 vegetation liquid water from space. *Remote Sensing of Environment* 58(3), 257-266.

725

726 Grueber, C. E., Nakagawa, S., Laws, R. J., & Jamieson, I. G. (2011). Multimodel
727 inference in ecology and evolution: challenges and solutions: Multimodel inference.
728 *Journal of Evolutionary Biology*, 24(4), 699–711. <https://doi.org/10.1111/j.1420-9101.2010.02210.x>

730

731 Hamilton, S.K., Sippel, S. J., & Melack, J. M. (1995). Oxygen depletion and carbon
732 dioxide and methane production in waters of the Pantanal wetland of Brazil.

733 *Biogeochemistry*, 30(2), 115-141. <https://doi.org/10.1007/BF00002727>

734
735
736
737
738
739
740
741
742
743
744
745
746
747
748
749
750
751
752
753
754

Hamilton, Stephen K., Sippel, S. J., Calheiros, D. F., & Melack, J. M. (1997). An anoxic event and other biogeochemical effects of the Pantanal wetland on the Paraguay River. *Limnology and Oceanography*, 42(2), 257–272.

<https://doi.org/10.4319/lo.1997.42.2.0257>

Happell, J. D., & Chanton, J. P. (1993). Carbon remineralization in a north Florida swamp forest: Effects of water level on the pathways and rates of soil organic matter decomposition. *Global Biogeochemical Cycles*, 7(3), 475–490.

<https://doi.org/10.1029/93GB00876>

Hess, L. L., Melack, J. M., Affonso, A. G., Barbosa, C., Gastil-Buhl, M., & Novo, E. M. L. M. (2015). Wetlands of the lowland Amazon basin: Extent, vegetative cover, and dual-season inundated area as mapped with JERS-1 synthetic aperture radar. *Wetlands*, 35(4), 745–756. <https://doi.org/10.1007/s13157-015-0666-y>

Ho, D. T., Engel, V. C., Ferrón, S., Hickman, B., Choi, J., & Harvey, J. W. (2018). On factors influencing air-water gas exchange in emergent wetlands. *Journal of Geophysical Research: Biogeosciences*, 123(1), 178–192.

<https://doi.org/10.1002/2017JG004299>

755 Junk, W. J., Bayley, P. B., & Sparks, R. E. (1989). The flood pulse concept in river-
756 floodplain systems. *Canadian special publication of fisheries and aquatic sciences*,
757 *106*(1), 110-127.

758
759 Junk, W.J., Piedade, M., Wittman, F., Schöngart, J. and Parolin, P. (eds.) (2010).
760 *Amazonian floodplain forests: ecophysiology, biodiversity and sustainable management*.
761 Dordrecht [Netherlands] ; New York: Springer.

762
763 Kasper, D., Amaral, J. H. F., & Forsberg, B. R. (2018). The effect of filter type and
764 porosity on total suspended sediment determinations. *Analytical Methods*. *10*, 5532-
765 5539. <https://doi.org/10.1039/C8AY02134A>

766
767 Kemenes, A., B.R. Forsberg and J.M. Melack. (2011). CO₂ emissions from a tropical
768 hydroelectric reservoir (Balbina, Brazil). *Journal of Geophysical Research- Biogeosciences*
769 *116*, G03004. <https://doi.org/10.1029/2010JG001465>

770
771 Lehner, B., & Döll, P. (2004). Development and validation of a global database of lakes,
772 reservoirs and wetlands. *Journal of Hydrology*, *296*(1–4), 1–22.
773 <https://doi.org/10.1016/j.jhydrol.2004.03.028>

774
775 MacIntyre, S., & Melack, J. M. (1995). Vertical and horizontal transport in lakes: linking
776 littoral, benthic, and pelagic habitats. *Journal of the North American Benthological*
777 *Society*, *14*(4), 599–615. <https://doi.org/10.2307/1467544>

778

779 MacIntyre, S., R. Wanninkhof, & J. Chanton (1995). Trace gas exchange across the air-
780 water interface in freshwater and coastal marine environments. Chapter 3 in (P.
781 Matson and R. Harriss, eds.) *Biogenic Trace Gases: Measuring Emissions from Soil
782 and Water*. Blackwell. pp. 52-97.

783

784 MacIntyre, S., Romero, J. R., & Kling, G. W. (2002). Spatial-temporal variability in
785 surface layer deepening and lateral advection in an embayment of Lake Victoria, East
786 Africa. *Limnology and Oceanography*, 47(3), 656–671.

787 <https://doi.org/10.4319/lo.2002.47.3.0656>

788

789 MacIntyre, S., Crowe, A. T., Cortés, A., & Arneborg, L. (2018). Turbulence in a small
790 arctic pond. *Limnology and Oceanography*, 63(6), 2337–2358.

791 <https://doi.org/10.1002/lno.10941>

792

793 MacIntyre, S., Amaral, J.H.F., Barbosa, P.M., Cortés, A., Forsberg, B.R. and Melack,
794 J.M. (2019). Turbulence and gas transfer velocities in sheltered flooded forests of the
795 Amazon basin. *Geophysical Research Letters* 46, 9628–9636. [https://doi.org/10.1029/
796 2019GL083948](https://doi.org/10.1029/2019GL083948)

797

798 Marengo, J. A., & Espinoza, J. C. (2016). Extreme seasonal droughts and floods in
799 Amazonia: causes, trends and impacts. *International Journal of Climatology*, 36(3),
800 1033–1050. <https://doi.org/10.1002/joc.4420>

801

802 Melack, J. M. (2016). Aquatic Ecosystems. In L. Nagy, B. R. Forsberg, & P. Artaxo
803 (Eds.), *Interactions Between Biosphere, Atmosphere and Human Land Use in the*
804 *Amazon Basin* (pp. 119–148). Berlin, Heidelberg: Springer Berlin Heidelberg.
805 https://doi.org/10.1007/978-3-662-49902-3_7

806

807 Melack, J. M., & Forsberg, B.R. (2001). Biogeochemistry of Amazon floodplain. In M.E.
808 McClain, R.L. Victoria and J.E. Richey (Eds.) *The Biogeochemistry of the Amazon*
809 *Basin and its Role in a Changing World* (pp. 235-276). Oxford University Press: New
810 York, NY, USA

811

812 Melack, J.M., & Engle, D. (2009). An organic carbon budget for an Amazon floodplain
813 lake. *Internationale Vereinigung für Theoretische und Angewandte Limnologie:*
814 *Verhandlungen* 30(8), 1179–1182. <https://doi.org/10.1080/03680770.2009.11923906>

815

816 Melack, J. M., & Hess, L. L. (2010). Remote sensing of the distribution and extent of
817 wetlands in the Amazon basin. In W. J. Junk, M. T. F. Piedade, F. Wittmann, J.
818 Schöngart, & P. Parolin (Eds.), *Amazonian Floodplain Forests* (pp. 43–59). Dordrecht:
819 Springer Netherlands. https://doi.org/10.1007/978-90-481-8725-6_3

820

821 Melack, J. M., Hess, L. L., Gastil, M., Forsberg, B. R., Hamilton, S. K., Lima, I. B. T., &
822 Novo, E. M. L. M. (2004). Regionalization of methane emissions in the Amazon Basin

823 with microwave remote sensing. *Global Change Biology*, 10(5), 530–544.

824 <https://doi.org/10.1111/j.1365-2486.2004.00763.x>

825

826 Melack, J. M., Novo, E. M. L. M., Forsberg, B. R., Piedade, M. T. F., & Maurice, L.

827 (2009). Floodplain ecosystem processes. In M. Keller, M. Bustamante, J. Gash, & P.

828 Silva Dias (Eds.), *Geophysical Monograph Series* (Vol. 186, pp. 525–541). Washington,

829 D. C.: American Geophysical Union. <https://doi.org/10.1029/2008GM000721>

830

831 Moreira-Turcq, P., Bonnet, M.-P., Amorim, M., Bernardes, M., Lagane, C., Maurice, L.,

832 et al. (2013). Seasonal variability in concentration, composition, age, and fluxes of

833 particulate organic carbon exchanged between the floodplain and Amazon River.

834 *Global Biogeochemical Cycles*, 27(1), 119–130. <https://doi.org/10.1002/gbc.20022>

835

836 Mortillaro, J. M., Passarelli, C., Abril, G., Hubas, C., Alberic, P., Artigas, L. F., et al.

837 (2016). The fate of C4 and C3 macrophyte carbon in central Amazon floodplain waters:

838 Insights from a batch experiment. *Limnologia*, 59, 90–98.

839 <https://doi.org/10.1016/j.limno.2016.03.008>

840

841 Pangala, S. R., Enrich-Prast, A., Basso, L. S., Peixoto, R. B., Bastviken, D., Hornibrook,

842 E. R. C., et al. (2017). Large emissions from floodplain trees close the Amazon methane

843 budget. *Nature*, 552 (7684), 230–234. <https://doi.org/10.1038/nature24639>

844

845 Parolin, P., Wittmann, F., Schöngart, J. (2010). Tree phenology in Amazonian floodplain
846 forests. In W. J. Junk, M. T. F. Piedade, F. Wittmann, J. Schöngart, & P. Parolin (Eds.),
847 *Amazonian Floodplain Forests* (pp. 106–126). Dordrecht: Springer Netherlands.

848 https://doi.org/10.1007/978-90-481-8725-6_5

849

850 Piedade, M.T.F., Ferreira, C.S., Oliveira Wittmann, A., Buckeridge, M, & Parolin P.
851 (2010a). Biochemistry of Amazonian floodplain trees. In W. J. Junk, M. T. F. Piedade, F.
852 Wittmann, J. Schöngart, & P. Parolin (Eds.), *Amazonian Floodplain Forests* (pp. 127–
853 139). Dordrecht: Springer Netherlands. https://doi.org/10.1007/978-90-481-8725-6_6

854

855 Piedade, M. T. F., Junk, W., D`Ângelo, S. A., Wittmann, F., Schöngart, J., Barbosa, K.
856 M. do N., & Lopes, A. (2010b). Aquatic herbaceous plants of the Amazon floodplains:
857 state of the art and research needed. *Acta Limnologica Brasiliensia*, 22(2), 165–178.

858 <https://doi.org/10.4322/actalb.02202006>

859

860 Pinel, S., Bonnet, M.-P., Santos Da Silva, J., Moreira, D., Calmant, S., Satgé, F., &
861 Seyler, F. (2015). Correction of interferometric and vegetation biases in the SRTMGL1
862 spaceborne DEM with hydrological conditioning towards improved hydrodynamics
863 modeling in the Amazon basin. *Remote Sensing*, 7(12), 16108–16130.

864 <https://doi.org/10.3390/rs71215822>

865

866 Poindexter, C. M., Baldocchi, D. D., Matthes, J. H., Knox, S. H., & Variano, E. A. (2016).
867 The contribution of an overlooked transport process to a wetland's methane emissions.

868 *Geophysical Research Letters*, 43(12), 6276–6284.

869 <https://doi.org/10.1002/2016GL068782>

870

871 Polsenaeere, P., Deborde, J., Detandt, G., Vidal, L. O., Pérez, M. A. P., Marieu, V., &

872 Abril, G. (2013). Thermal enhancement of gas transfer velocity of CO₂ in an Amazon

873 floodplain lake revealed by eddy covariance measurements. *Geophysical Research*

874 *Letters*, 40(9), 1734–1740. <https://doi.org/10.1002/grl.50291>

875

876 Pulliam, W. M. (1993). Carbon dioxide and methane exports from a southeastern

877 floodplain swamp. *Ecological Monographs*, 63(1), 29–53.

878 <https://doi.org/10.2307/2937122>

879

880 Quay, P. D., Wilbur, D., Richey, J. E., Hedges, J. I., Devol, A. H., & Victoria, R. (1992).

881 Carbon cycling in the Amazon River: Implications from the ¹³C compositions of particles

882 and solutes. *Limnology and Oceanography*, 37(4), 857–871.

883 <https://doi.org/10.4319/lo.1992.37.4.0857>

884

885 Rasera, de F. M., Krusche, A. V., Richey, J. E., Ballester, M. V. R., & Victória, R. L.

886 (2013). Spatial and temporal variability of pCO₂ and CO₂ efflux in seven Amazonian

887 Rivers. *Biogeochemistry*, 116(1–3), 241–259. [https://doi.org/10.1007/s10533-013-9854-](https://doi.org/10.1007/s10533-013-9854-0)

888 [0](https://doi.org/10.1007/s10533-013-9854-0)

889

890 Raymond, P. A., Hartmann, J., Lauerwald, R., Sobek, S., McDonald, C., Hoover, M., et
891 al. (2013). Global carbon dioxide emissions from inland waters. *Nature*, 503(7476),
892 355–359. <https://doi.org/10.1038/nature12760>

893
894 Richey, J. E., Devol, A. H., Wofsy, S. C., Victoria, R., & Riberio, M. N. G. (1988).
895 Biogenic gases and the oxidation and reduction of carbon in Amazon River and
896 floodplain waters: Amazon dissolved gases. *Limnology and Oceanography*, 33(4), 551–
897 561. <https://doi.org/10.4319/lo.1988.33.4.0551>

898
899 Richey, J. E., Hedges, J. I., Devol, A. H., Quay, P. D., Victoria, R., Martinelli, L., &
900 Forsberg, B. R. (1990). Biogeochemistry of carbon in the Amazon River. *Limnology and*
901 *Oceanography*, 35(2), 352–371. <https://doi.org/10.4319/lo.1990.35.2.0352>

902
903 Richey, J. E., Melack, J. M., Aufdenkampe, A. K., Ballester, V. M., & Hess, L. L. (2002).
904 Outgassing from Amazonian rivers and wetlands as a large tropical source of
905 atmospheric CO₂. *Nature*, 416(6881), 617–620. <https://doi.org/10.1038/416617a>

906
907 Rudorff, C. M., Melack, J. M., MacIntyre, S., Barbosa, C. C. F., & Novo, E. M. L. M.
908 (2011). Seasonal and spatial variability of CO₂ emission from a large floodplain lake in
909 the lower Amazon. *Journal of Geophysical Research*, 116(G04007).
910 <https://doi.org/10.1029/2011JG001699>

911

912 Sawakuchi, H. O., Neu, V., Ward, N. D., Barros, M. de L. C., Valerio, A. M., Gagne-
913 Maynard, W., et al. (2017). Carbon dioxide emissions along the lower Amazon River.
914 *Frontiers in Marine Science*, 4. <https://doi.org/10.3389/fmars.2017.00076>
915

916 Sorribas, M. V., Paiva, R. C. D., Melack, J. M., Bravo, J. M., Jones, C., Carvalho, L., et
917 al. (2016). Projections of climate change effects on discharge and inundation in the
918 Amazon basin. *Climatic Change*, 136(3–4), 555–570. [https://doi.org/10.1007/s10584-](https://doi.org/10.1007/s10584-016-1640-2)
919 [016-1640-2](https://doi.org/10.1007/s10584-016-1640-2)
920

921 Strickland, J. D., & Parsons, T. R. (1972). *A practical handbook of seawater analysis*.
922 Fisheries Research Board of Canada, Ottawa, 310 p.
923

924 Tathy, J. P., Cros, B., Delmas, R. A., Marengo, A., Servant, J., & Labat, M. (1992).
925 Methane emission from flooded forest in central Africa. *Journal of Geophysical*
926 *Research*, 97(D6), 6159-6168. <https://doi.org/10.1029/90JD02555>
927

928 Tedford, E. W., MacIntyre, S., Miller, S. D., & Czikowsky, M. J. (2014). Similarity scaling
929 of turbulence in a temperate lake during fall cooling. *Journal of Geophysical Research:*
930 *Oceans*, 119(8), 4689–4713. <https://doi.org/10.1002/2014JC010135>
931

932 Valderrama, J. C. (1981). The simultaneous analysis of total nitrogen and total
933 phosphorus in natural waters. *Marine Chemistry*, 10(2), 109–122.
934 [https://doi.org/10.1016/0304-4203\(81\)90027-X](https://doi.org/10.1016/0304-4203(81)90027-X)

935
936
937
938
939
940
941
942
943
944
945
946
947
948
949
950
951
952
953
954
955

Waichman, A. V. (1996). Autotrophic carbon sources for heterotrophic bacterioplankton in a floodplain lake of central Amazon. *Hydrobiologia*, 341(1), 27–36.

<https://doi.org/10.1007/BF00012300>

Wanninkhof, R. (1992). Relationship between wind speed and gas exchange over the ocean. *Journal of Geophysical Research*, 97(C5), 7373.

<https://doi.org/10.1029/92JC00188>

Ward, N. D., Keil, R. G., Medeiros, P. M., Brito, D. C., Cunha, A. C., Dittmar, T., et al. (2013). Degradation of terrestrially derived macromolecules in the Amazon River.

Nature Geoscience, 6(7), 530–533. <https://doi.org/10.1038/ngeo1817>

Ward, N. D., Bianchi, T. S., Sawakuchi, H. O., Gagne-Maynard, W., Cunha, A. C., Brito, D. C., et al. (2016). The reactivity of plant-derived organic matter and the potential importance of priming effects along the lower Amazon River. *Journal of Geophysical Research: Biogeosciences*, 121(6), 1522–1539. <https://doi.org/10.1002/2016JG003342>

Weiss, R. F., & Price, B. A. (1980). Nitrous oxide solubility in water and seawater.

Marine Chemistry, 8(4), 347–359. [https://doi.org/10.1016/0304-4203\(80\)90024-9](https://doi.org/10.1016/0304-4203(80)90024-9)

956 Wiesenburg, D. A., & Guinasso, N. L. (1979). Equilibrium solubilities of methane, carbon
957 monoxide, and hydrogen in water and sea water. *Journal of Chemical & Engineering*
958 *Data*, 24(4), 356–360. <https://doi.org/10.1021/je60083a006>

959
960 Wittmann, F., Anhuf, D., & Funk, W. J. (2002). Tree species distribution and community
961 structure of central Amazonian várzea forests by remote-sensing techniques. *Journal of*
962 *Tropical Ecology*, 18(6), 805–820. <https://doi.org/10.1017/S0266467402002523>

963
964 Wittmann, F., Schöngart, J., & Junk, W. J. (2010). Phytogeography, species diversity,
965 community structure and dynamics of central Amazonian floodplain forests. In W. J.
966 Junk, M. T. F. Piedade, F. Wittmann, J. Schöngart, & P. Parolin (Eds.), *Amazonian*
967 *Floodplain Forests* (pp. 61–102). Dordrecht: Springer Netherlands. .
968 https://doi.org/10.1007/978-90-481-8725-6_4

969
970 Worbes, M., Klinge, H., Revilla, J. D., & Martius, C. (1992). On the dynamics, floristic
971 subdivision and geographical distribution of várzea forests in Central Amazonia. *Journal*
972 *of Vegetation Science*, 3(4), 553–564. <https://doi.org/10.2307/3235812>

973
974 Worbes, M. (1997). The Forest Ecosystem of the Floodplains. In W. J. Junk (Ed.), *The*
975 *Central Amazon Floodplain: Ecology of a Pulsing System* (pp. 223–265). Berlin,
976 Heidelberg: Springer Berlin Heidelberg. https://doi.org/10.1007/978-3-662-03416-3_11

977
978 Zappa, C. J., McGillis, W. R., Raymond, P. A., Edson, J. B., Hintsä, E. J., Zemmeling,

979 H. J., et al. (2007). Environmental turbulent mixing controls on air-water gas exchange
980 in marine and aquatic systems. *Geophysical Research Letters*, 34, L10601.

981 <https://doi.org/10.1029/2006GL028790>

982

983

984

985

986

987

988

989

990

991

992

993

994

995

996

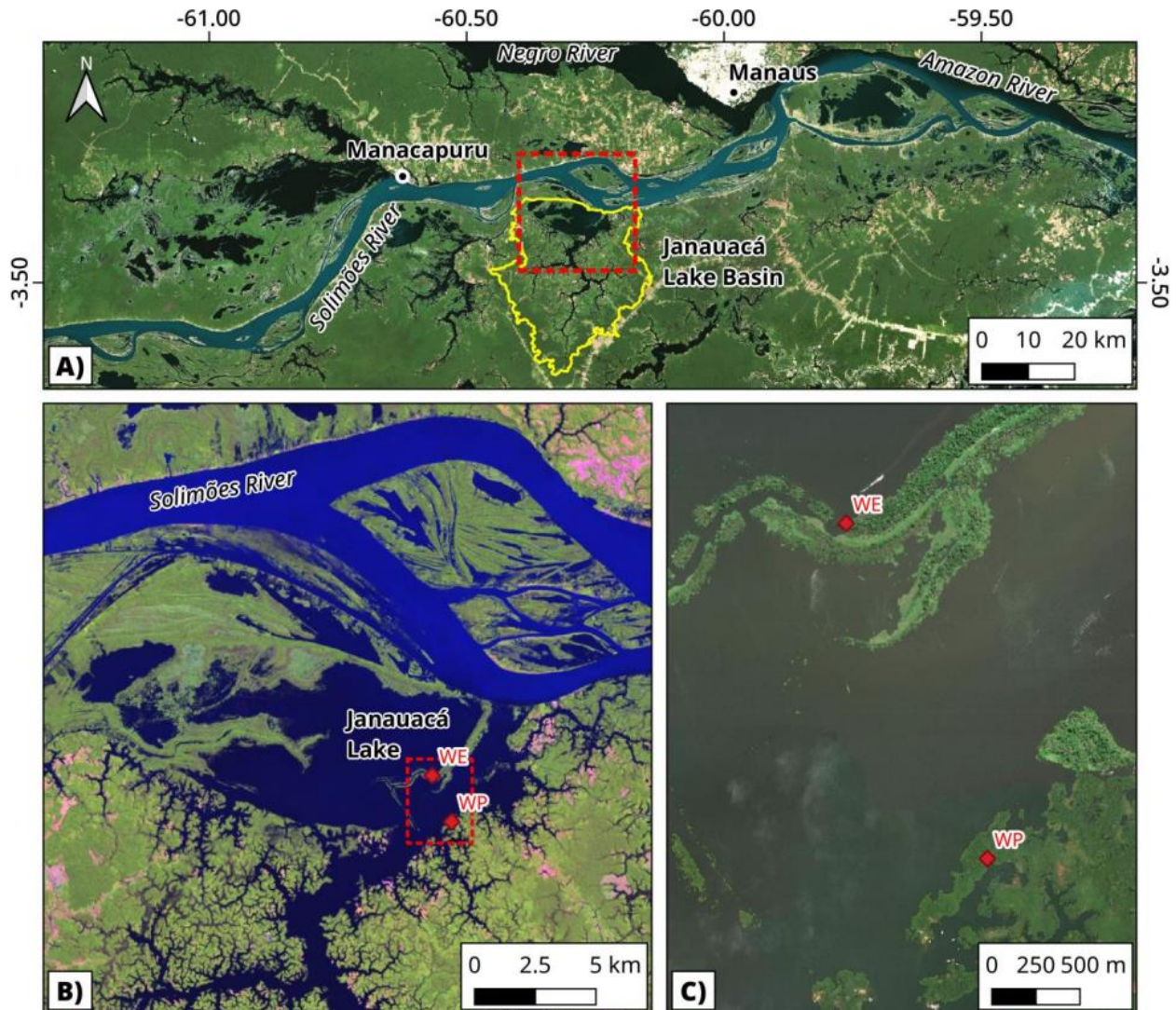
997

998

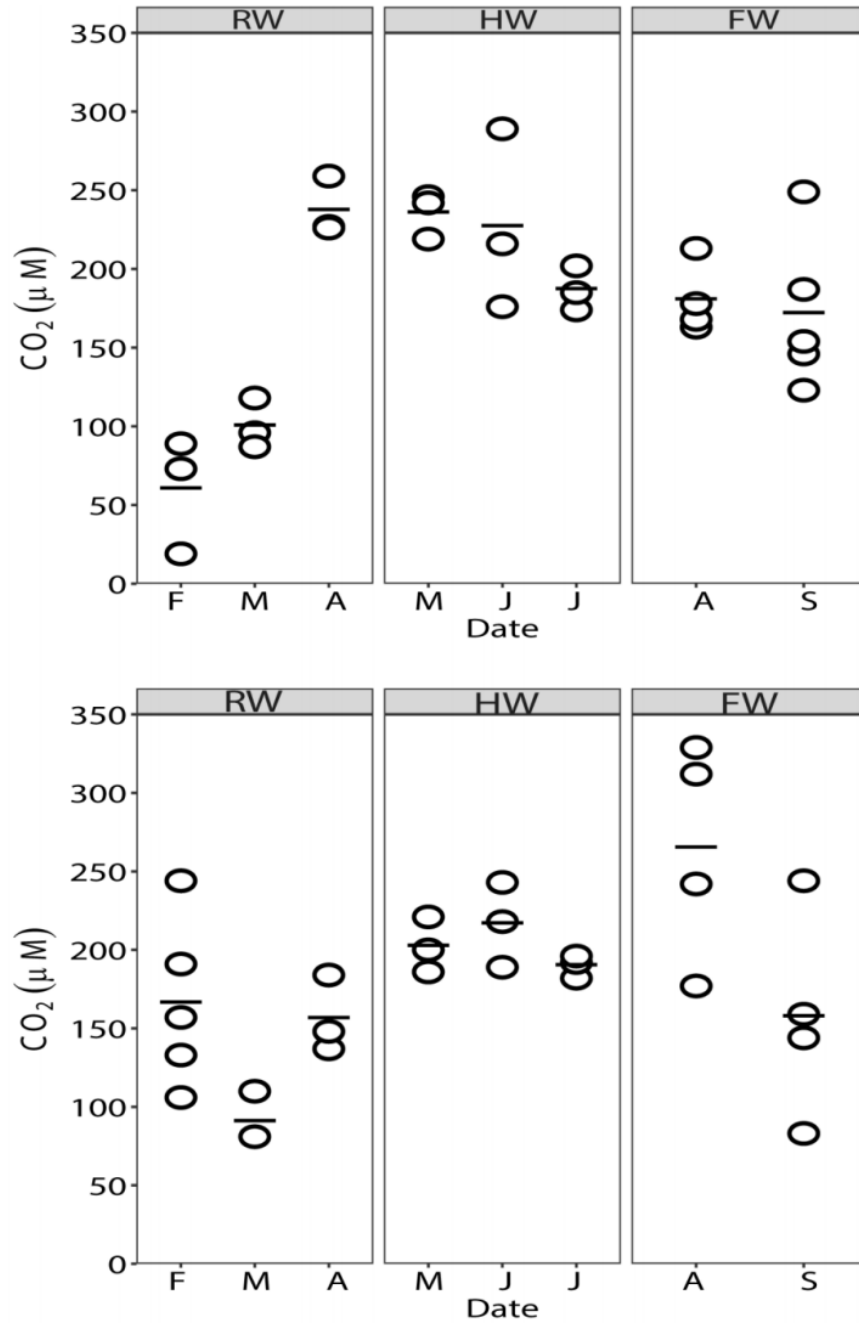
999

1000

1001

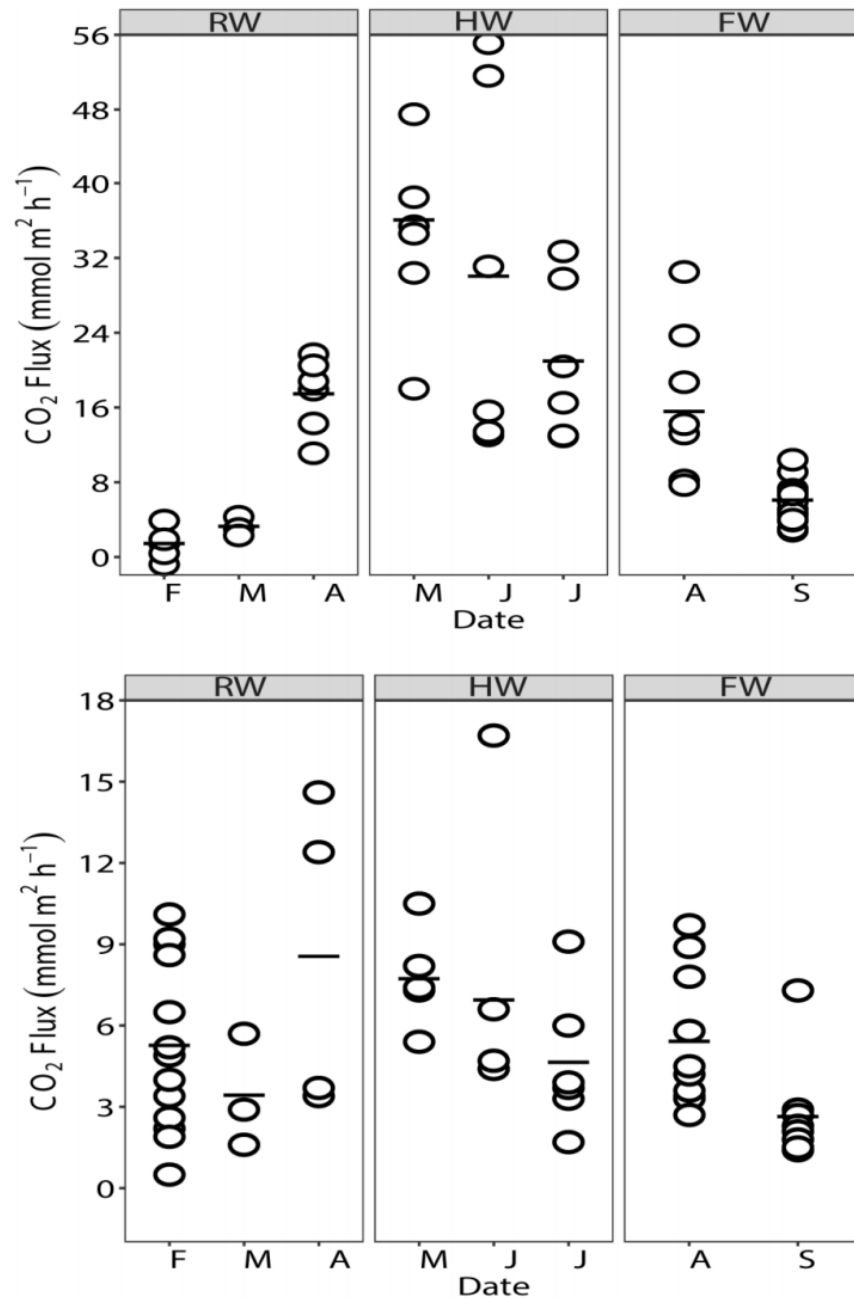


1003
 1004 **Figure 1.** A) General location of the study site showing the watershed (yellow line)
 1005 (Background: ESRI World Imagery). B) Composite high-water Landsat 8 image showing
 1006 the upper Janauacá floodplain (red dashed) (R5,G4,B3). C) Location of the sampled
 1007 flooded forest sites: wind exposed site (WE) and wind protected site (WP). Red dashed
 1008 lines indicate the boundaries of the following figure panel. Janauacá lake basin
 1009 delimited by Pinel et al. (2015).



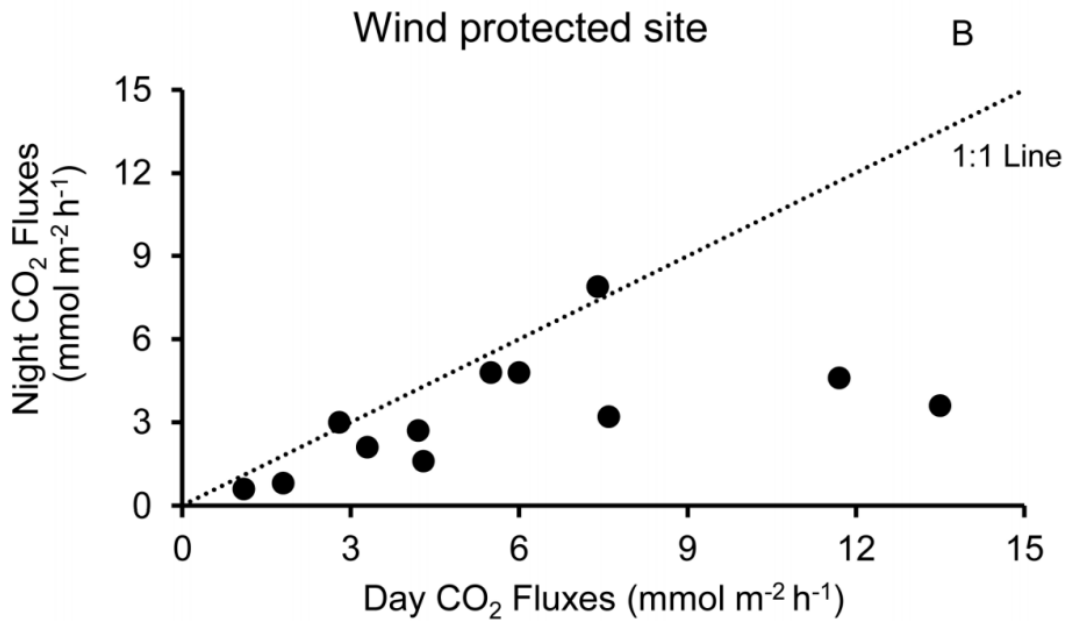
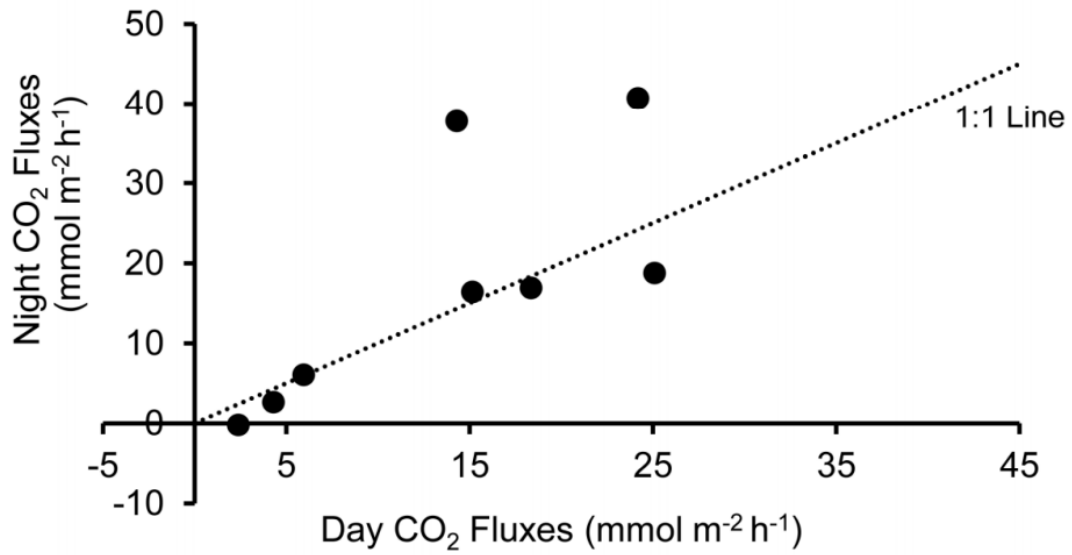
1011

1012 **Figure 2.** CO₂ concentrations measured at the wind exposed site (WE, upper panel)
 1013 and wind protected site (WP, lower panel) during the study and divided into hydrological
 1014 periods: rising water (RW), high water (HW) and falling water (FW). Horizontal bars
 1015 represent the mean per sampling date, open circles represent each observation in a 24
 1016 h period.



1017

1018 **Figure 3.** CO₂ evasion measured at the wind exposed site (WE, upper panel) and wind
 1019 protected site (WP, lower panel) during the study and divided by hydrological period:
 1020 rising water (RW), high water (HW) and falling water (FW). Horizontal bars represent
 1021 the mean, open circles represent each observation in a 24 h period. Note differences in
 1022 scale of y axis between sites.



1023

1024

Figure 4. Mean CO₂ fluxes measured during the night versus measurements made

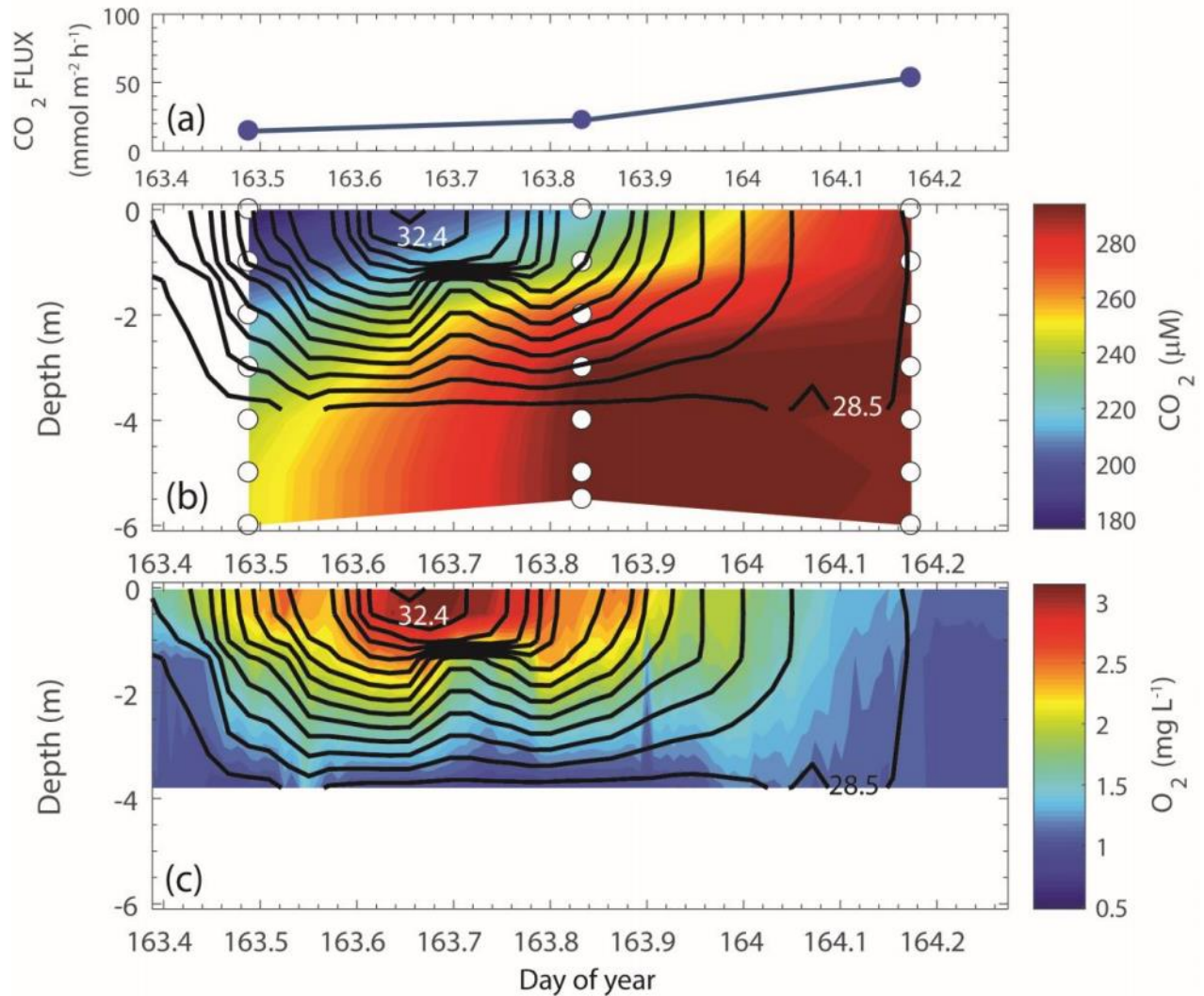
1025

during the day for the wind exposed (A) and protected (B) sites. Dashed lines represent

1026

the 1:1 equivalence

1027



1028

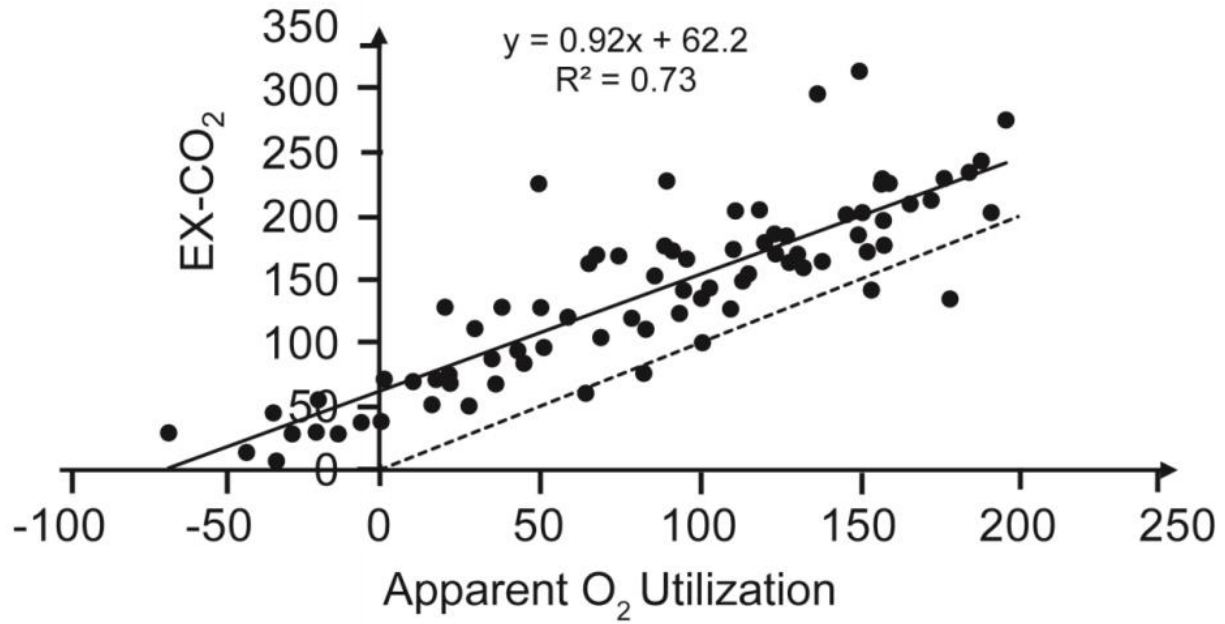
1029 **Figure 5.** Upper panel) Time series of CO₂ fluxes, Middle panel) Dissolved CO₂
 1030 concentrations from discrete measurements at depths indicated by white dots, and
 1031 Lower Panel) 10 min averaged time series of dissolved oxygen in the wind exposed
 1032 flooded forest in June 2015. Hourly averaged isotherms at 0.3°C intervals are shown as
 1033 black contours with maximum and minimum isotherms labelled.

1034

1035

1036

1037



1038

1039 **Figure 6.** Excess of CO₂ as function of apparent oxygen utilization (AOU) in μM,
1040 calculated for the surface waters of inundated forests investigated in our study. Dashed
1041 line is the 1:1 line and solid black line is the regression line.

Table 1. Surface CO₂ concentrations, flux and gas transfer velocities (k_{600}) measured in wind exposed (WE) and wind protected (WP) flooded forests. SD is the standard deviation; Min/max indicates the minimum and maximum values among the n measurements on each date.

PERIOD	MONTH	CO ₂ (μM)		CO ₂ Flux (mmol m ⁻² h ⁻¹)		K ₆₀₀ (cm h ⁻¹)	
		WP Mean, SD (Min/max, n)	WE Mean, SD (Min/max, n)	WP Mean, SD (Min/max, n)	WE Mean, SD (Min/max, n)	WP Mean, SD (Min/max, n)	WE Mean, SD (Min/max, n)
Falling Water	Aug 2014	158 ± 43 (112/ 216, 5)		2.8 ± 1.2 (0.9 / 4.6,13)		1.5 ± 0.7 (0.4 / 2.6, 13)	
Rising Water	Feb 2015	166 ± 53 (106 / 244, 5)	61 ± 37 (19/ 89, 3)	5.2 ± 3.2 (0.5/ 10.1, 13)	1.4 ± 1.8 (-0.8* / 3.9, 5)	2.5 ± 1.1 (0.3 / 4.2, 13)	4.1 ± 2.5 (1.7 / 8.0, 5)
	March 2015	90 ± 17 (81 / 110, 3)	100 ± 16 (87 / 118, 3)	3.4 ± 2.1 (1.6 / 5.7, 3)	3.2 ± 1.0 (2.3 / 4.3, 3)	3.3 ± 1.4 (1.8 / 4.5, 3)	2.9 ± 1.1 (1.8 / 4, 3)
	April 2015	156 ± 24 (137 / 184, 3)	237 ± 19 (226 / 259, 3)	8.5 ± 5.8 (3.4/ 14.6, 4)	17 ± 4.0 (11 / 22, 6)	5.3 ± 4.0 (1.8 / 9.5, 4)	6.4 ± 1.8 (3.7 / 8.3, 6)
High Water	May 2015	202 ± 17 (186 / 221, 3)	236 ± 15 (219 / 246, 3)	7.7 ± 1.7 (5.4 / 10.5, 6)	36 ± 10 (18 / 48, 7)	3.2 ± 0.6 (2.3 / 4, 6)	12.8 ± 3.5 (6.8 / 16.8, 7)
	June 2015	217 ± 27 (189/ 243, 3)	227 ± 57 (177 / 289, 3)	6.9 ± 4.9 (4.4 / 16.7, 6)	30 ± 19 (13 / 55, 6)	2.6 ± 1.8 (1.6 / 6.2, 6)	10 ± 4.8 (4.9 / 16, 6)
	July 2015	190 ± 7 (182 / 196, 3)	187 ± 14 (174 / 202, 3)	4.6 ± 2.6 (1.7 / 9.1, 6)	30 ± 8.5 (13 / 33, 6)	2.1 ± 1.2 (0.8 / 4.2, 6)	9.7 ± 4.2 (5.6 / 15, 6)
Falling Water	Aug 2015	265 ± 70 (177 / 329, 4)	180 ± 22 (163 / 213, 4)	5.4 ± 2.5 (2.7 / 9.7, 10)	16 ± 8.3 (8 / 31, 8)	1.6 ± 1.1 (0.7 / 4.3, 10)	7.4 ± 4.7 (2.9 / 16, 8)
	Sept 2015	157 ± 66 (83/ 244, 4)	172 ± 49 (123 / 250, 5)	2.6 ± 1.8 (1.4 / 7.3, 9)	6 ± 2.1 (3 / 10, 17)	2.1 ± 1.9 (0.7 / 6.9, 9)	3.3 ± 2.3 (1.3 / 8.3, 17)
High Water	July 2016	111 ± 36 (80 / 164, 5)		3.6 ± 1.2 (2.1 / 5.4, 10)		3.1 ± 1.6 (1.8 / 5.9, 10)	
Falling Water	Aug 2016	55 ± 13 (41 / 70, 5)		1.0 ± 0.3 (0.5 / 1.3, 11)		1.7 ± 0.3 (1.4 / 2.3, 11)	
	Sept 2016	94 ± 66 (24/ 203, 10)		1.7 ± 1.3 (0.1 / 4.8, 21)		1.9 ± 1.4 (0.2 / 6, 21)	

*The in-gassing value was measured under high Chl-*a* concentrations; 18 μgL^{-1} in the flooded forest and 25 μgL^{-1} in associated open waters, suggesting that Chl-*a* enriched water was advected from the open waters to the flooded forest site. We had one replicate measurement with negative flux and another with a positive flux, but both with high r^2 (>0.95). When replicates were averaged, the value was still negative.

Table 2. Average CO₂ diffusive fluxes (FCO₂) measured within flooded forests from different studies.

Location	Forest Type	Method	FCO ₂ mg C m ⁻² d ⁻¹
Amazon basin ^a	Floodplain	chamber	343
Florida USA ^b	Swamp	chamber	973 ± 599
Georgia, USA ^c	Floodplain	chamber	115 – 1270*
Congo basin ^d	Floodplain	chamber	2640 ± 1370
Pantanal, Brazil ^e	Floodplain	modeled	320
Northern Australia ^f	Floodplain	chamber	1260 ± 1258
Amazon basin ^g	Floodplain	chamber	2182 ± 2954

^a Devol et al., 1988. Mean value calculated from nine measurements made during the high-water period.

^b Happell & Chanton, 1993. Mean value calculated from single daytime measurements once a month for one year.

^c Pulliam, 1993. *Range of mean daily fluxes obtained from ten transects with three measurements done at a monthly frequency for a two-year period.

^d Tathy et al., 1992. Mean value from eleven daily measurements made in flooded forests.

^e Dalmagro et al., 2018. Mean value obtained using 40 measurements of surface CO₂ water concentrations and a wind-based equation during the flooded season (March to June).

^f Bass et al., 2014. Mean value obtained from seven sites with daily replicate measurements done eight times during the flood season (February to May).

^g This study - Mean value from two sites with multiple measurements over diel cycles in 12 monthly campaigns distributed through two hydrological years when the forest sites were flooded and accessible.